Analysis and Sizing for Transient Thermal Heating of Insulated Aerospace Vehicle Structures

Max L. Blosser
Langley Research Center, Hampton, Virginia

NASA STI Program . . . in Profile

Since its founding, NASA has been dedicated to the advancement of aeronautics and space science. The NASA scientific and technical information (STI) program plays a key part in helping NASA maintain this important role.

The NASA STI program operates under the auspices of the Agency Chief Information Officer. It collects, organizes, provides for archiving, and disseminates NASA's STI. The NASA STI program provides access to the NASA Aeronautics and Space Database and its public interface, the NASA Technical Report Server, thus providing one of the largest collections of aeronautical and space science STI in the world. Results are published in both non-NASA channels and by NASA in the NASA STI Report Series, which includes the following report types:

- TECHNICAL PUBLICATION. Reports of completed research or a major significant phase of research that present the results of NASA Programs and include extensive data or theoretical analysis. Includes compilations of significant scientific and technical data and information deemed to be of continuing reference value. NASA counterpart of peer-reviewed formal professional papers, but having less stringent limitations on manuscript length and extent of graphic presentations.

- TECHNICAL MEMORANDUM. Scientific and technical findings that are preliminary or of specialized interest, e.g., quick release reports, working papers, and bibliographies that contain minimal annotation. Does not contain extensive analysis.

- CONTRACTOR REPORT. Scientific and technical findings by NASA-sponsored contractors and grantees.

- CONFERENCE PUBLICATION. Collected papers from scientific and technical conferences, symposia, seminars, or other meetings sponsored or co-sponsored by NASA.

- SPECIAL PUBLICATION. Scientific, technical, or historical information from NASA programs, projects, and missions, often concerned with subjects having substantial public interest.

- TECHNICAL TRANSLATION. English-language translations of foreign scientific and technical material pertinent to NASA's mission.

Specialized services also include organizing and publishing research results, distributing specialized research announcements and feeds, providing information desk and personal search support, and enabling data exchange services.

For more information about the NASA STI program, see the following:

- Access the NASA STI program home page at *http://www.sti.nasa.gov*

- E-mail your question to help@sti.nasa.gov

- Fax your question to the NASA STI Information Desk at 443-757-5803

- Phone the NASA STI Information Desk at 443-757-5802

- Write to:
  STI Information Desk
  NASA Center for AeroSpace Information
  7115 Standard Drive
  Hanover, MD 21076-1320

Analysis and Sizing for Transient Thermal Heating of Insulated Aerospace Vehicle Structures

Max L. Blosser
Langley Research Center, Hampton, Virginia

August 2012

Acknowledgments

Abstract

An analytical solution was derived for the transient response of an insulated structure subjected to a simplified heat pulse. The solution is solely a function of two nondimensional parameters. Simpler functions of these two parameters were developed to approximate the maximum structural temperature over a wide range of parameter values. Techniques were developed to choose constant, effective thermal properties to represent the relevant temperature and pressure-dependent properties for the insulator and structure. A technique was also developed to map a time-varying surface temperature history to an equivalent square heat pulse. Equations were also developed for the minimum mass required to maintain the inner, unheated surface below a specified temperature. In the course of the derivation, two figures of merit were identified. Required insulation masses calculated using the approximate equation were shown to typically agree with finite element results within 10%-20% over the relevant range of parameters studied.

Nomenclature

a_1, a_2 Coefficients of approximate equation for maximum structural temperature

b_n Coefficients of series solution for $\tau > \tau_h$

c_m Coefficients of series solution for $0 < \tau \leq \tau_h$

c_{pe} Effective insulator specific heat capacity

c_{ps} Structural specific heat capacity

d_e Insulator thickness

d_s Structural thickness

f_{thr} Fraction of the surface temperature range

k_e Effective insulator thermal conductivity

m Mass per unit area

m_e Insulation mass per unit area

m_s Structural mass per unit area

m_{opt} Minimum total mass per unit area

m_{so} Structural mass/area at which total mass/area is minimum

P_{avg} Average ambient pressure during equivalent square surface temperature pulse

T Temperature

t Time

T_h	Applied surface temperature rise of insulator
t_h	Duration of heating pulse
T_i	Initial temperature
T_m	Maximum structural temperature rise
T_{ce}	Temperature to use for calculating effective insulation specific heat capacity
T_{cs}	Temperature to use for calculating effective structural specific heat capacity
T_{ha}	Applied surface temperature of insulator
T_{ke}	Temperature to use for calculating effective insulation conductivity
T_{ma}	Maximum structural temperature
T_{mx}	Maximum surface temperature for a surface temperature history
T_{thr}	Threshold temperature for truncating insulator temperature rise integral
x	Nondimensionalized spatial variable
x'	Spatial variable, position through insulator thickness
β	Ratio of insulator conductance/area to insulator heat capacity/area
β_s	Figure of merit for thermal performance of structure
δ	Dirac delta function
ϵ	Error of approximate equation
γ	Ratio of insulator to structural heat capacity/area
κ_e	Figure of merit for thermal performance of insulator
λ	Eigenvalue
ρ_e	Effective insulator density
ρ_s	Structural density
τ	Nondimensionalized time
τ_h	Nondimensionalized duration of heat pulse
τ_m	Nondimensionalized time of maximum structural temperature
θ	Nondimensionalized temperature

1 Introduction

Thermal protection systems are a critical component of hypersonic and atmospheric entry vehicles. The reusable ceramic tiles and blankets of the Space Shuttle Orbiter work well as thermal insulators, but result in a fragile, high maintenance exterior surface. An intriguing approach to this problem is to build the thermal insulation into the exterior vehicle wall. This deceptively simple idea will be difficult to achieve because it requires a flight weight aerospace vehicle skin to not only carry the required mechanical loads, but also to accommodate severe transient heating with the corresponding hot outer surface and large temperature gradients through its thickness.

A thermally insulating structural panel will likely be of a sandwich construction as a result of both thermal and structural considerations. The outer, heated face sheet of the sandwich will typically be a thin layer of non-insulating material that will contribute little to the thermal response of the inner, unheated face sheet. Thus, ignoring edge closeouts and joints, the transient thermal response of an insulating sandwich panel will be similar in character to the thermal response of an insulated structure like the external tiles and blankets covering the aluminum structure of the Space Shuttle Orbiter. For a non-homogeneous sandwich core, it may be possible to calculate effective thermal properties using a rule of mixtures to approximate its thermal performance.

In this paper, a simplified transient thermal problem was investigated in an attempt to gain basic insight that will be required to develop optimum sandwich panels that can simultaneously insulate and carry structural loads. An analytical solution was derived for the transient response of an insulated structure to a simplified heat pulse. The solution is a function of two nondimensional quantities. Simpler functions of these two parameters were developed to approximate the maximum structural temperature over a wide range of parameter values. Techniques were developed to choose constant, effective properties to represent the relevant temperature and time-dependent thermal properties for the insulator and structure. A technique was also developed to map a time-varying surface temperature history to an equivalent square heat pulse. Using these techniques, the maximum structural temperature rise was calculated using the analytical solutions and compared with finite element simulations over a wide range of parameters. Equations were also developed for the minimum mass for an insulated structure required to maintain the inner, unheated surface below a specified temperature. A figure of merit which correlates to the effectiveness of the heat capacity of the underlying structural material in reducing the amount of required insulation was developed. A second figure of merit was identified for the combination of insulator thermal properties that minimizes the mass of an insulator required to limit the maximum temperature of an underlying structure subjected to a transient heating pulse. Insulation was sized for a number of surface heating histories, insulators, and structural materials by iterating a one-dimensional, finite element analysis and by using the simple equations derived in this paper. Finite element results were correlated to the two figures of merit developed in this paper.
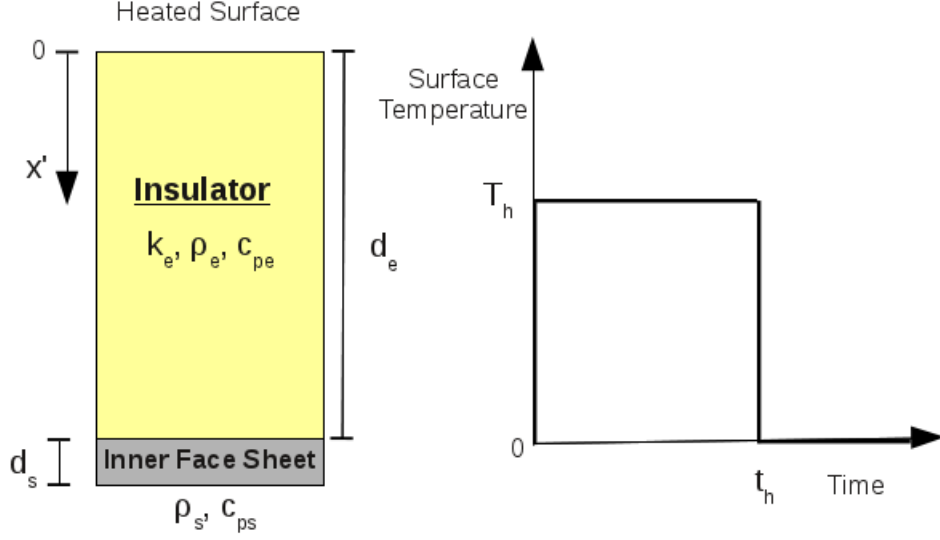
Figure 1. Illustration of simplified problem

2 Problem Definition

The simplified problem investigated in this paper is illustrated in Fig. 1. A thermal insulator with thickness, d_e, density, ρ_e, specific heat capacity, c_{pe}, and thermal conductivity, k_e, covers a structure (inner face sheet) of thickness, d_s, density, ρ_s, and specific heat capacity, c_{ps}. The inner surface of the structure is assumed to be perfectly insulated to simplify the mathematics of the problem and because it is a commonly used conservative assumption for sizing thermal protection systems. To further simplify the problem, the structure is treated as a lumped heat capacitance and the outer face sheet of the insulating sandwich panel is neglected. For this solution, the material properties are assumed to be constant, so effective, averaged properties would have to be used to approximate more complex material behavior.

A simple transient heat pulse is assumed. Initially the insulator and structure are assumed to be at a uniform temperature of 0. The outer surface of the insulator is assumed to instantaneously rise to a temperature T_h at $t = 0$ and maintain that temperature until $t = t_h$ at which time it instantaneously returns to 0.

2.1 Mathematical Description

Using a nondimensional spatial variable, $x = \frac{x'}{d_e}$, the governing differential equation for heat conduction through the insulator can be written as

$$\frac{\partial T}{\partial t} = \beta \frac{\partial^2 T}{\partial^2 x} \tag{1}$$

where

$$\beta = \frac{k_e}{\rho_e c_{pe} d_e^2} \tag{2}$$

4

The boundary condition at $x = 1$ is defined as

$$\frac{\partial T(1, t)}{\partial t} = -\beta\gamma\frac{\partial T(1, t)}{\partial x} \tag{3}$$

where

$$\gamma = \frac{\rho_e c_{pe} d_e}{\rho_s c_{ps} d_s} \tag{4}$$

The boundary condition at $x = 0$ is defined as

$$T(0, t) = \begin{cases} T_h & \text{for } 0 < t \le t_h \\ 0 & \text{for } t > t_h \end{cases} \tag{5}$$

Finally, the initial condition is a uniform temperature of 0.

$$T(x, 0) = 0 \tag{6}$$

The mathematical problem defined by Eqs. 1 through 6 can be completely nondimensionalized [1] by defining a nondimensional time, $\tau = \beta t$ and a nondimensional temperature, $\theta = \frac{T}{T_h}$. The nondimensionalized differential equation becomes

$$\frac{\partial\theta}{\partial\tau} = \frac{\partial^2\theta}{\partial^2 x} \tag{7}$$

The boundary condition at $x = 1$ becomes

$$\frac{\partial\theta(1, \tau)}{\partial\tau} = -\gamma\frac{\partial\theta(1, \tau)}{\partial x} \tag{8}$$

The boundary condition at $x = 0$ becomes

$$\theta(0, \tau) = \begin{cases} 1 & \text{for } 0 < \tau \le \tau_h \\ 0 & \text{for } \tau > \tau_h \end{cases} \tag{9}$$

where

$$\tau_h = \frac{k_e}{\rho_e c_{pe} d_e^2} t_h \tag{10}$$

The initial condition becomes

$$\theta(x, 0) = 0 \tag{11}$$

2.2 Nondimensional Governing Parameters

Inspection of the mathematical problem defined by Eqs. 7 through 11 reveals that any solution will be completely governed by two nondimensional parameters, γ and τ_h. Each of these parameters has clear physical significance. The first parameter, γ, is defined by Eq. 4 which shows it to be the ratio of the heat capacity per unit area of the insulator to the heat capacity per unit area of the underlying structure.

Equation 10 defining the nondimensional heat pulse duration, τ_h, can be slightly rewritten to show that it is the ratio of insulator conductance per unit area to heat capacity per unit area times the duration of the heat pulse. The same ratio of

insulator conductance per unit area to heat capacity per unit area, β, is used to nondimensionalize time.

$$\tau_h = \frac{\frac{k_e}{d_e}}{\rho_e c_{pe} d_e} t_h \tag{12}$$

3   Analytical Solution

An analytical solution for the problem illustrated in Fig. 1 can be obtained by combining two existing solutions with modifications. The solution of the first part of the problem, $0 < t \le t_h$, can be found in the classic heat transfer textbook by Carslaw and Yeager [2]. Converting the solution to the nomenclature used in this paper and nondimensionalizing produces

$$\theta(x,\tau) = \frac{T(x,\tau)}{T_h} = 1 - \sum_{m=1}^{\infty} c_m \sin(\lambda_m x) e^{-\lambda_m^2 \tau} \tag{13}$$

where

$$c_m = \frac{2(\lambda_m^2 + \gamma^2)}{\lambda_m(\lambda_m^2 + \gamma^2 + \gamma)} \tag{14}$$

The values for λ_m can be found by solving the equation

$$\lambda_m \tan \lambda_m = \gamma \tag{15}$$

Solving the second part of the problem, $t > t_h$, requires more effort. There is an existing solution for a similar problem in which the insulator and lumped mass are initially at a uniform temperature, but at $t = 0$ the temperature of the insulator outer surface is instantaneously reduced to 0. A solution to this similar problem, including its derivation, is presented in Reference [3]. A derivation of the solution to the second part of the current problem is presented in Appendix A. The derivation closely follows the approach used by De Chant, however, instead of a uniform temperature, the solution to Eq. 13 at time t_h is used as the initial temperature distribution.

So, for $t > t_h$ or $\tau > \tau_h$ the solution is

$$\theta(x,\tau) = \frac{T(x,\tau)}{T_h} = \sum_{n=1}^{\infty} b_n \sin(\lambda_n x) e^{-\lambda_n^2(\tau - \tau_h)} \tag{16}$$

where

$$b_n = c_n(1 - e^{-\lambda_n^2 \tau_h}) - \sum_{\substack{m=1 \\ m \ne n}}^{\infty} \left(\frac{\frac{\sin(\lambda_m - \lambda_n)}{(\lambda_m - \lambda_n)} - \frac{\sin(\lambda_m + \lambda_n)}{(\lambda_m + \lambda_n)} + \frac{2 \sin \lambda_m \sin \lambda_n}{\gamma}}{1 - \frac{\sin(2\lambda_n)}{2\lambda_n} + \frac{2 \sin^2 \lambda_n}{\gamma}} \right) c_m e^{(-\lambda_m^2 \tau_h)} \tag{17}$$

6

The quantities c_m and c_n can be calculated using Eq. 14 and values for λ_m and λ_n are obtained by solving Eq. 15. In Eq. 17 the summation excludes the term $m = n$ because the contribution of that term is captured by the exponential term preceding the summation.

4   Numerical Example for Series Solution

The series solution described by Eqs. 13 and 16 can be applied to a wide range of physical situations. However, the motivation for deriving the solution was to gain insight into the thermal response of an insulated structure of an aerospace vehicle subjected to a transient aerodynamic heating pulse. Therefore a numerical example was chosen to represent a typical location on the Space Shuttle Orbiter at which the aluminum structure is protected from aerodynamic heating by an LI-900 ceramic tile. The material properties, obtained from Reference [4], are listed in Table 1 along with dimensions, heating duration and the corresponding nondimensional parameters. Thermal properties are temperature dependent, so the properties for the aluminum structure are for $200°F$ and the properties for the LI-900 tile are for $1250°F$. The LI-900 thermal conductivity is also a strong function of pressure, so the conductivity is chosen for a pressure of 0.01 atm (an arbitrary value in the mid-range of a typical ambient pressure history for an atmospheric entry trajectory).

Table 1. Numerical values for initial example

Variable	Value	Units
d_s	0.125 (0.003175)	$in(m)$
ρ_s	175 (2800)	$lbm/ft^3(kg/m^3)$
c_{ps}	0.216 (904)	$Btu/lbm/°F(J/kg/K)$
d_e	2,3,4 (0.051,0.076, 0.102)	$in(m)$
ρ_e	9 (144)	$lbm/ft^3(kg/m^3)$
c_{pe}	0.296 (1238)	$Btu/lbm/°F(J/kg/K)$
k_e	0.0492 (0.0851)	$Btu/ft/hr/°F(W/m/K)$
t_h	25 (1500)	$min(s)$

A computer program was written using Version 2.7 of the Python programming language to implement the series solution described by Eqs. 13 and 16. Routines from Version 0.9 of the SciPy programming library [5] were used for numerical solutions of nonlinear equations and fitting coefficients to nonlinear equations. For times just after an instantaneous change in surface temperature, many terms of the series solution were required for an accurate solution. However, for the results shown in Figs. 2 through 5, eight terms were used to calculate the coefficients b_n and three terms to calculate c_m. Use of additional terms produced negligible changes in the results. To generate results for the wide range of parameter values shown in Figs. 6, 7, 9, and 10, twelve terms each were used to calculate b_n and c_m to reduce the chance of truncation error.

Three different tile thicknesses, d_e in Table 1, are considered to gain understanding of the solution described by Eqs. 13 and 16. The nondimensional temperature distributions through the thickness of the insulator at several times are shown in Figs. 2, 3, and 4 for LI-900 tile thicknesses of 2, 3, and 4 in. (0.051,0.076, 0.102m) respectively. In each figure, the solid blue line represents the temperature distribution halfway through the heat pulse and the solid green line represents the temperature at the end of the heat pulse, $\tau = \tau_h$. The dashed lines represent temperature distributions after the heat pulse has ended, $\tau > \tau_h$. As expected the tile interior and underlying structure heats up more quickly and reaches a higher temperature for thinner tiles. Fig. 2 shows that the structure at $x = 1$ has already started heating up midway through the heating pulse, $\tau = \frac{\tau_h}{2} = 0.14$ for a tile thickness of 2 inches. In contrast, Fig. 4 shows that the structure has not even started to heat up at the end of the heat pulse, $\tau = \tau_h = 0.07$ for a tile thickness of 4 in. This behavior is expected because it should take much longer for the heat to diffuse through twice the thickness of tile.
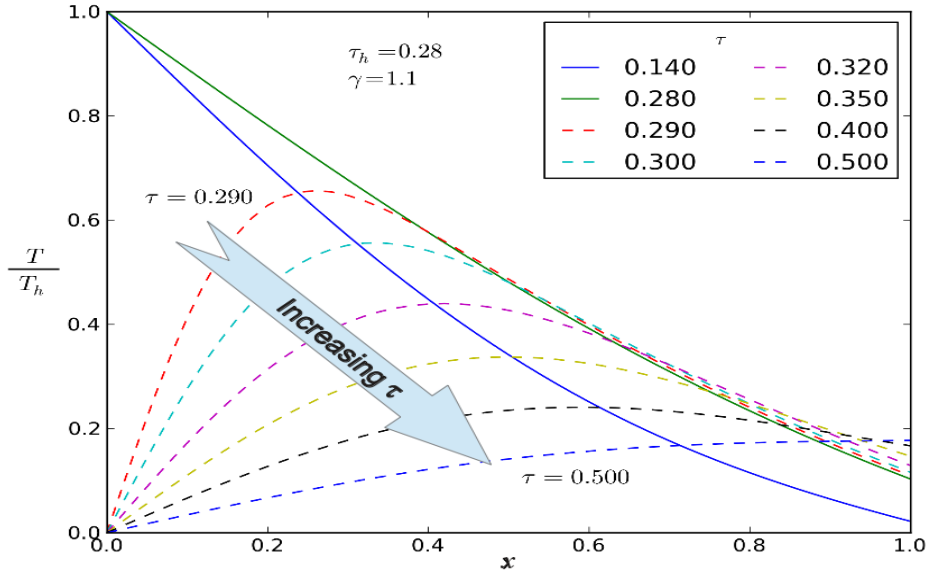

Figure 2. Temperature distributions for 2 inch thick tile

After the tile surface temperature drops back to the initial temperature, the heat stored in the tile interior begins to be conducted back out of the cooled outer tile surface. However, the underlying structure, $x = 1$, continues to increase in temperature until its temperature matches that of the tile material in contact with it, then it begins to cool. This behavior is consistent with the assumption that the structure is perfectly insulated on its inner surface.

For sizing of thermal protection systems, the temperature of the underlying structure is of primary concern. Further insight into the solution can be obtained by calculating the structural temperature as a function of time. Figure 5 shows a
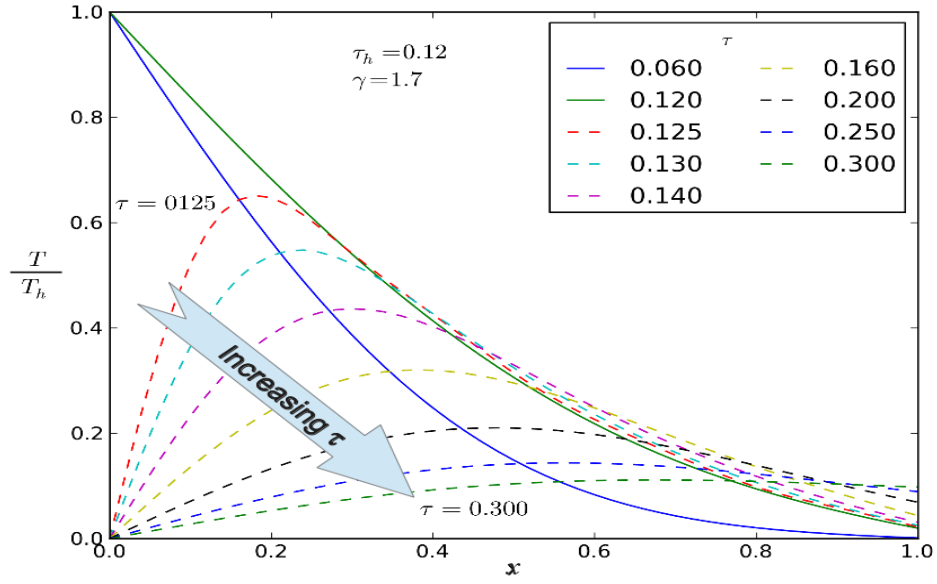
Figure 3. Temperature distributions for 3 inch thick tile

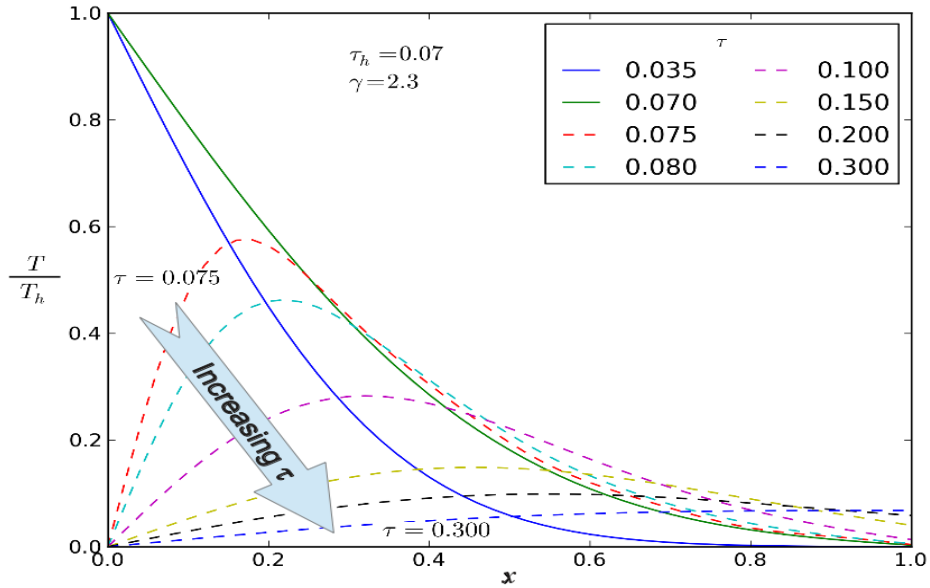Figure 4. Temperature distributions for 4 inch thick tile

number of temperature histories for different combinations of the governing nondi-mensional parameters. The ranges of the two parameters were chosen to bound the values calculated for the numerical examples illustrated in Figs. 2 through 4. In Fig. 5, the blue lines represent the structural temperature histories for $\tau_h = 0.05$, the
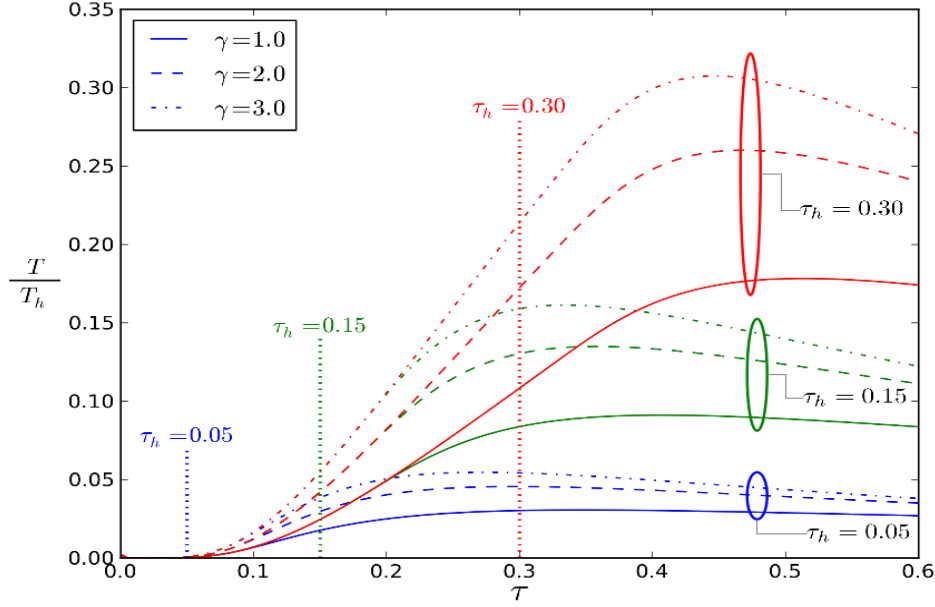
9

Figure 5. Structural temperature histories as a function of governing parameters

green for $\tau_h = 0.15$, and the red for $\tau_h = 0.3$. The vertical dotted lines represent the end of the heat pulse for the respective values of τ_h. The solid, dashed and dash-dot lines represent values of γ of 1, 2, and 3 respectively. Because the nondimensionalized time axis makes the results more difficult to interpret physically, it is helpful to consider the case of fixed material properties and heating duration. The remaining free parameters would be the insulator thickness, d_e, and the structural thickness, d_s. The parameter τ_h varies as $\frac{1}{d_e^2}$, so smaller values of τ_h imply larger values of d_e. Choosing a value of τ_h fixes the insulator thickness, so for a specified value of τ_h, γ can only be varied by changing the structural thickness. The parameter γ varies as $\frac{1}{d_s}$ so larger values of γ imply smaller structural thicknesses. In Fig. 5 the structural temperature histories for $\tau_h = 0.05$ stay much cooler, which is consistent with the expected behavior for thicker insulation. Conversely the structural temperatures reach much higher values for $\tau_h = 0.3$, which is consistent with the expected behavior for thinner insulation. For each value of τ_h the curve for $\gamma = 1$ reaches the lowest maximum temperature, as expected for the correspondingly highest structural heat capacity. Higher γ's result in higher maximum structural temperatures as expected for the associated reduction in structural heat capacity. All of the structural temperature history curves in Fig. 5 exhibit similar behavior. The temperature of the structure continues to rise well after completion of the heating pulse, reaches a maximum value, and then begins to decrease. The maximum temperature is a primary design driver for sizing of thermal protection systems, so it is desirable to be able to readily calculate the maximum structural temperature.

10

5   Maximum Structural Temperature

All of the temperature histories, away from the heated surface, generated using Eq. 16 would appear to heat up, reach a maximum temperature, and then begin to cool. The time at which the maximum temperature occurs can be found by differentiating Eq. 16 with respect to time, setting it equal to zero, and solving for time. This results in the following equation to be solved for τ_m

$$0 = -\sum_{n=1}^{\infty} \lambda_n^2 b_n \sin(\lambda_n x) e^{-\lambda_n^2 (\tau_m - \tau_h)} \tag{18}$$

Equation 18 can be solved for the time of the maximum temperature for any location through the thickness of the insulator. However, for the current problem, the maximum structural temperature at $x = 1$ is of greatest interest. The equation therefore becomes

$$0 = -\sum_{n=1}^{\infty} \lambda_n^2 b_n \sin(\lambda_n) e^{-\lambda_n^2 (\tau_m - \tau_h)} \tag{19}$$

Although Eq. 19 cannot be readily solved for τ_m in closed form, it can be solved numerically. The nondimensional times at which the maximum structural temperature occurs for a range of the governing parameters are shown in Fig. 6.
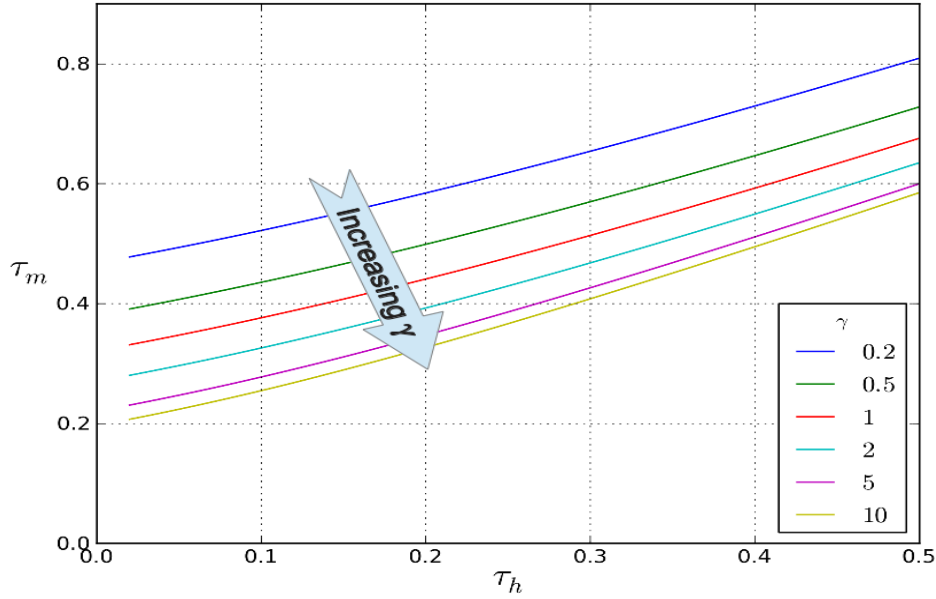

Figure 6. Times at which maximum structural temperatures occur

The resulting τ_m can be substituted into Eq. 16 to obtain the maximum structural temperature rise. Following this procedure, the maximum structural temperature rise was calculated over a range of the governing nondimensional parameters

$(0.2 \leq \gamma \leq 5$ and $0.02 \leq \tau_h \leq 0.5)$. Figure 7 shows a surface plot of the maximum structural temperature rises calculated over a 49 by 49 point grid. The color contours from dark blue to red indicate increasing maximum structural temperature rises. To gain insight into the physical implications of this plot it is again helpful to consider the case of fixed material properties. For fixed properties, small values of τ_h imply a short heat pulse and/or thick insulator and large values imply a long heat pulse and/or thin insulator. It is logical to expect that as the heat pulse duration goes to zero, $\tau_h \to 0$, the maximum structural temperature rise will also go to zero. The parameter, γ, is the ratio of insulation to structural heat capacity per unit area, so small values imply that the structural heat capacity per unit area is much larger than that of the insulation and large values imply a relatively small amount of structural heat capacity. Therefore, as the structural heat sink increases towards infinity, γ will approach 0 and, for a finite heating duration, the maximum structural temperature rise will also go to zero. Also, for this problem, the maximum structural temperature cannot exceed the applied surface temperature, so $\frac{T_m}{T_h} \leq 1$.
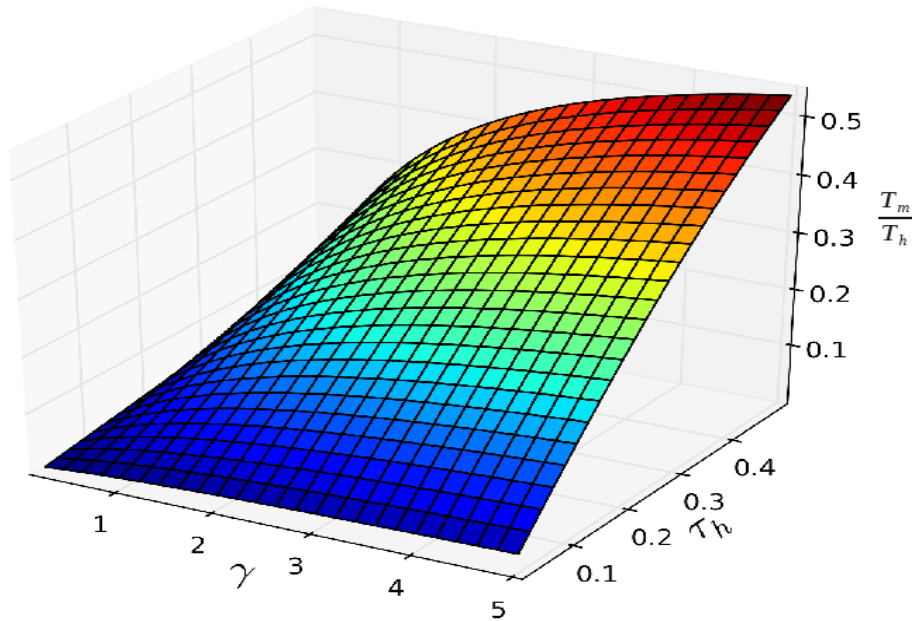
Figure 7. Maximum structural temperatures

The maximum structural temperature rise plot in Fig. 7 is useful to illustrate how the maximum structural temperature rise varies with the two governing parameters, but it was generated using a complicated series of numerical solutions. For quick calculations, it would be much more useful to have a relatively simple algebraic equation to approximate this surface. The approximate solution should go to zero if either of the governing parameters goes to zero, and it should approach 1 as either parameter goes to infinity. A number of candidate equations were evaluated and the following approximate solution was chosen as a good compromise between simplicity and accuracy.

12

$$\left(\frac{T_m}{T_h}\right)_a = 1 - e^{(a_1 \gamma^{a_2} \tau_h{}^{2a_2})} \tag{20}$$

where the subscript a indicates approximate.

A "least squares" routine was used to find the values of the coefficients in Eq. 20 that best approximate the surface shown in Fig. 7. The coefficient values are given in Table 2.

Table 2. Coefficient values for Eq. 20

Coefficient	Value
a_1	-0.72058
a_2	0.53649

Inspection of Table 2 reveals that $a_1 \approx \frac{-1}{\sqrt{2}}$ and $a_2 \approx \frac{1}{2}$. Substituting these coefficients into Eq. 20 simplifies the equation to

$$\left(\frac{T_m}{T_h}\right)_a = 1 - e^{-\tau_h \sqrt{\frac{\gamma}{2}}} \tag{21}$$

The approximate maximum structural temperature rises calculated using Eq. 20 with the coefficient values listed in Table 2 are shown in Fig. 8. The plot is similar to that in Fig. 7.
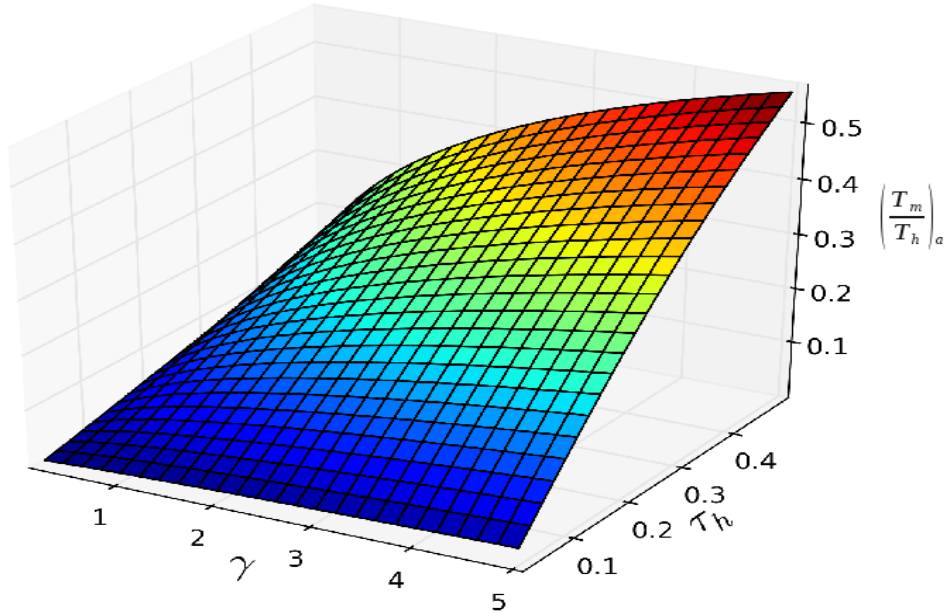
Figure 8. Approximate maximum structural temperatures

The values from Fig. 7 were subtracted from those of Fig. 8 to calculate the absolute errors resulting from the approximation.

$$\epsilon_a = \left(\frac{T_m}{T_h}\right)_a - \frac{T_m}{T_h} \tag{22}$$

Figure 9 shows the distribution of error over the previously chosen range of governing parameters. Over much of the surface errors are within $\pm 1\%$ of the applied surface temperature rise, T_h. Highest errors occur for small values of γ and large values of τ_h.
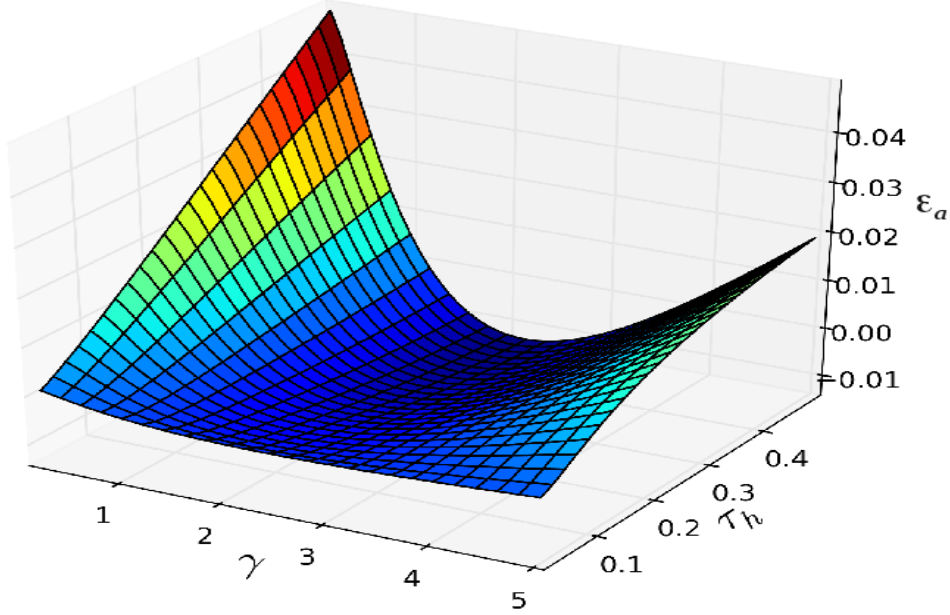
Figure 9. Errors using approximate maximum structural temperature equation

It may be more instructive to consider the relative error distribution. The relative errors between the approximation of Eq. 20 and the series solution were calculated using the following equation

$$\epsilon_r = \frac{\left(\frac{T_m}{T_h}\right)_a - \frac{T_m}{T_h}}{\frac{T_m}{T_h}} \tag{23}$$

Figure 10 shows the distribution of the relative error over the previously chosen range of governing parameters. Over most of the parameter space, the relative error is within $\pm 10\%$. For small values of γ, however, the relative error rises precipitately. Therefore it would be prudent to check the values of γ for any calculations made using Eq. 20 to avoid the inaccurate region. This inaccurate region of the approximate solution corresponds to a physical situation where the structural skin is much heavier than the insulator.
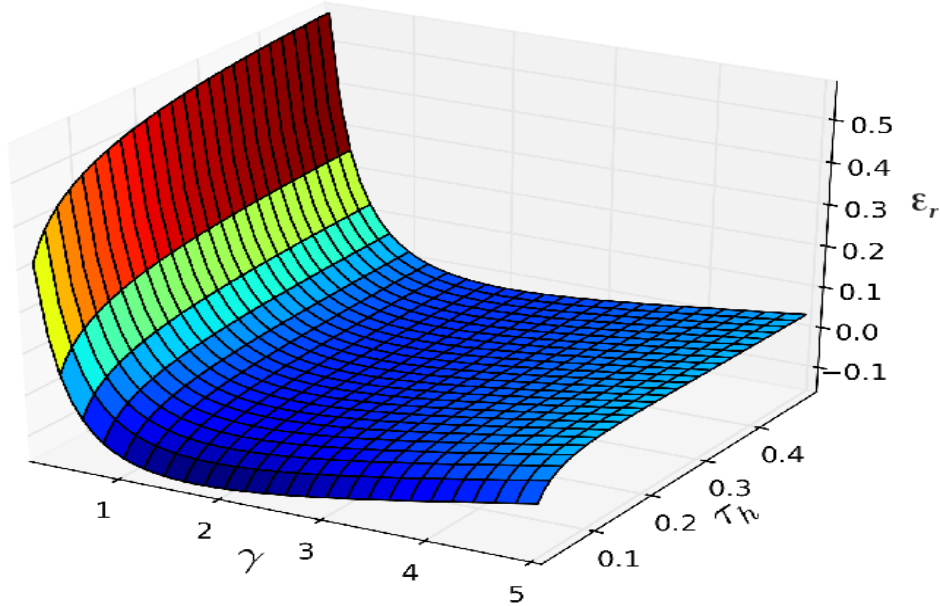
Figure 10. Relative errors using approximate maximum structural temperature equation

6   Comparison of Analytical and Numerical Solutions

The problem illustrated in Fig. 1 is considerably simpler than a typical numerical simulation of aerodynamic heating of an insulated aerospace vehicle structure. Material properties, which can vary with temperature and pressure, are treated as constant. The applied surface temperature is a simple square pulse, rather than a more realistic transient profile. A numerical model was developed to: 1) demonstrate that the series solution, Eqs. 13 and 16, produces the expected results, 2) verify that the governing nondimensional parameters (γ and τ_h), rather than individual material property values, determine the calculated temperatures, 3) develop techniques for best using the analytical solution to approximate a realistic numerical simulation, and 4) estimate typical errors involved in using the analytical solution to approximate a realistic numerical simulation.

6.1   Numerical Model

A one-dimensional finite element model was developed using the DOLFIN [6] finite element library for the Python programming language. Using the DOLFIN library, linear one dimensional elements were used to discretize the spatial dimension and an implicit Crank-Nicolson time marching scheme was used to solve the weak formulation of the diffusion equation. The model consisted of a layer of insulator material in perfect contact with a layer of structural material similar to the configuration shown in Fig. 1, except that the structure in the finite element model was

not treated as a lumped heat capacitance. For the results shown in this paper, the model consisted of 50 elements through the thickness of the insulator and 2 elements through the thickness of the structure. Although a careful convergence study was not performed, a model with half the number of elements was shown to produce nearly identical results. The boundary condition on the outer surface of the insulator consisted of an imposed surface temperature that could be varied arbitrarily with time and updated at each time step of the solution. The inner surface of the structure was adiabatic. The material properties could be arbitrary functions of temperature and ambient pressure. Material property values for each finite element were updated at each time step of the analysis for the average temperature of each element from the previous time step. Property values could be different for each element, but did not vary spatially within an element. Time steps between 1 and 5 seconds were used to calculate the results presented in this paper.

When comparing results from the finite element and analytical solutions it is important to understand and correctly handle a subtle difference in how the two solutions treat temperature. Because material properties are constant, the analytical solution deals strictly with temperature rise from a uniform initial temperature (assumed to be zero for simplicity in the derivation). Therefore, T_h and T_m have been defined for the analytical solution as maximum temperature rise for the insulator surface and structure, respectively. For the numerical solutions, however, absolute temperatures must be used so that the solution is able to look up the correct temperature dependent material properties. Therefore, it is helpful to define two more variables to clarify this distinction in subsequent discussions.

$$T_{ma} = T_m + T_i$$
$$T_{ha} = T_h + T_i$$
(24)

6.2   Simplified Problem

A finely discretized finite element model of the problem illustrated in Fig. 1 should give exactly the same answer as the analytical series solution defined by Eqs. 13 and 16. Both solution techniques solve the same differential equation with the same boundary and initial conditions.

A numerical example, using the properties, dimensions, and heating values given in Table 1, was studied with the previously described finite element model and the series solution. A thickness of 3 inches for the LI-900 insulation, an initial temperature of $60°F$ and an applied surface temperature, T_{ha}, of $2000°F$ were chosen to complete the problem definition. Calculated temperature distributions at several times are shown in Fig. 11. This solution is the same as that shown in nondimensional form in Fig. 3. The symbols in Fig. 11 represent the temperatures calculated at each node of the finite element model. The solid lines represent the series solution defined by Eqs. 13 and 16. The blue and green circles represent distributions halfway through and at the end of the heating pulse, respectively. The triangular symbols represent temperature distributions at several times after the heat pulse has

ended. The finite element and series solutions are essentially in exact agreement, as expected.
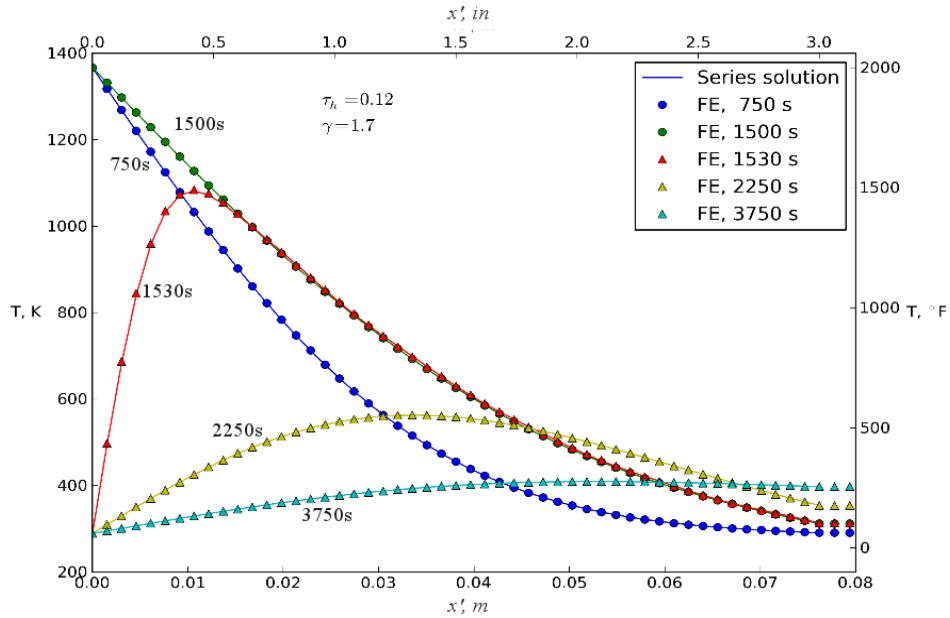
Figure 11. Temperature distributions from finite element model vs series solution

The primary concern for thermal protection system sizing is the maximum structural temperature. Figure 12 shows the calculated temperature history of the structure. Again the finite element analysis (temperature gradients in the structure were negligible) and the series solution are essentially in exact agreement, as expected. The red square shown in Fig. 12 was obtained by solving Eq. 19 for the time of maximum structural temperature and substituting that value into Eq. 16 to calculate the maximum structural temperature. The green circle represents the approximate maximum structural temperature calculated using Eq. 20, which is a temperature rise 6% lower than the exact answer.

As shown earlier in the mathematical formulation of the problem, any solution should depend only on the values of the nondimensional governing parameters and not the individual parameter values. A parametric study was performed using the finite element model to confirm that the numerical solution also depends only on the value of the nondimensional parameters. Results of the study are shown in Table 3. Again, the baseline properties are from Table 1 and were also used to generate Figs. 11 and 12. Numerical values of the governing nondimensional parameters and the maximum structural temperatures shown in Fig. 12 are presented in Table 3. For the parametric study, selected combinations of material properties, dimensions, and/or heating time were scaled so that the nondimensional parameter values remain unchanged. Even though individual parameter values were doubled or halved, the calculated maximum structural temperature was the same within 6 significant digits because the nondimensional parameter values were unchanged.

17
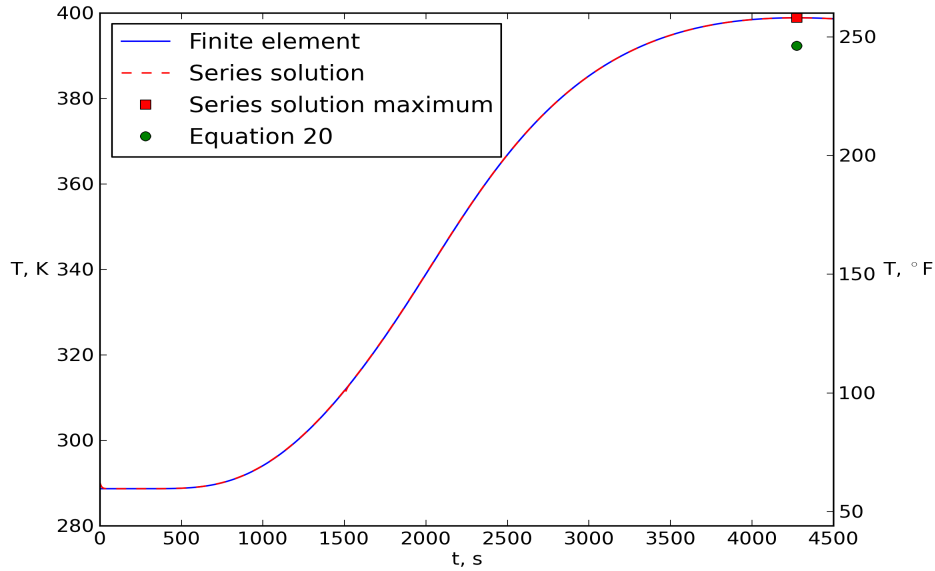
Figure 12. Structural temperature history from finite element model vs series solution

6.3 Material Property Variation

Constant material properties were assumed to obtain the analytical solution. However, the material properties can vary significantly during a transient heating pulse. The specific heat capacities of the structure and insulator, c_{ps} and c_{pe}, can vary significantly with temperature. The thermal conductivity of the insulator, k_e, can vary greatly with both temperature and ambient pressure. To investigate the effect of variable material properties, the temperature dependent specific heats of the aluminum structure and LI-900 insulation and the temperature and pressure dependent thermal conductivity of LI-900, Tables B1-B3 in Appendix B, were incorporated into the one-dimensional finite element model. In addition, the thermal model for heat transfer through flexible fibrous insulation from Reference [7] was incorporated into a Python computer program and used to predict the effective thermal conductivity of Saffil® insulation in air. The objective of the finite element analysis was to develop a rationale for choosing equivalent constant material properties for the analytical solution. The equivalent properties are chosen to approximate the effect of temperature- and pressure-dependent properties on the calculated maximum structural temperature. The effect of each variable material property was investigated separately with all other material properties held constant.

6.3.1 Structural Specific Heat Capacity

The structural specific heat capacity, c_{ps}, was investigated first because it was expected to be the easiest to understand. The structure undergoes the smallest

18

Table 3. Numerical study of nondimensional governing parameters

Governing Parameters		
$\gamma = 1.69032$, $\tau_h = 0.123318$		
Baseline maximum structural temperature, K		
Series	Eq. 20	Finite element
398.898	392.325	398.908
Parametric Study		
Scaled parameters	Scale factor	Max. str. temp., K
c_{ps}, c_{pe}, k_e	2.0	398.908
ρ_s, c_{pe}, k_e	2.0	398.908
c_{ps}, ρ_e, t_h	0.5	398.908
ρ_s, d_e, k_e, t_h	0.5	398.908

temperature change, is most isolated from the sharp temperature transients on the surface of the insulator, and undergoes relatively moderate changes in specific heat capacity as temperature varies. The obvious approach would be to use the specific heat capacity at the average of the maximum and initial structural temperatures. The previously described one dimensional finite element model was used to investigate the effect of temperature dependent c_{ps} on the calculated maximum structural temperature. The finite element analysis was the same as that used for the baseline results in Table 3, except that the constant value of c_{ps} was replaced by the temperature dependent values from Table B1. The results of the finite element analysis with temperature dependent c_{ps} are shown in Table 4. The second column shows the initial temperature, the average structural temperature, and the maximum structural temperature from the finite element analysis. The third column shows the value of the temperature dependent structural specific heat capacity for the initial, average, and maximum structural temperatures, respectively. The corresponding γ and τ_h are shown for each value of c_{ps}. These values of γ and τ_h were used to calculate the associated maximum structural temperatures using the series (Eq. 16) and approximate (Eq. 20) solutions. Comparing the quantities in bold faced type in Table 4, it is obvious that using c_{ps} for the average structural temperature in the series solution gives almost exactly (within 0.1%) the same answer as the finite element analysis with temperature dependent c_{ps}.

6.3.2 Insulator Specific Heat Capacity

The effect of temperature dependency of the insulator specific heat capacity, c_{pe}, on maximum structural temperature is a little more complicated. The insulator undergoes much larger temperature excursions than the structure and experiences large, transient temperature gradients whereas the structure has negligible gradients. It is not obvious which value of c_{pe} should be used in the analytical solutions to best match the finite element solution with temperature dependent c_{pe}. Again,

Table 4. Effect of temperature dependent structural specific heat capacity

Structural Temperature	Finite Element T, K	$c_{ps}(T)$ $\left(\frac{J}{kgK}\right)$	γ	τ_h	T_{ma}(Series) K	T_{ma}(Eq. 20) K
Initial	288.71	842.7	1.8134	0.12332	403.01	396.10
Average	344.33	886.7	1.7234	0.12332	**400.03**	**393.35**
Maximum	**399.95**	924.4	1.6530	0.12332	397.60	391.15
$t_h =$ **1500s** $T_{ha} =$**1366K**						

the same finite element model was used as that for the baseline results in Table 3, except that the constant value of c_{pe} was replaced by the temperature dependent values from Table B2. Finite element simulations were performed for two different values of maximum surface temperature and three different values of heating time. Results are presented in Table 5. For each simulation c_{pe} values for the insulator were calculated at three different temperatures: initial temperature, maximum structural temperature, and the average between the initial and maximum insulator temperatures. The associated values of the governing nondimensional parameters are shown for each value of c_{pe} along with the corresponding maximum structural temperatures calculated using the series and approximate solutions. Using the c_{pe} values at the maximum structural temperature in the analytical solutions most closely matched the finite element result, as indicated by the bold faced temperatures shown in Table 5 for each simulation. The series solution results are within $\pm 8\%$ of the structural temperature rise predicted by the finite element analysis of this limited set of cases. Therefore, using $c_{pe}(T_{ma})$ as a constant value in the analytical solutions may be an acceptable approach for approximating the effect of temperature dependent c_{pe} on maximum structural temperature.

6.3.3 Insulator Thermal Conductivity

Thermal conductivity of the insulator can be a strong function of both temperature and ambient pressure. For simplicity, the effects of pressure and temperature were considered separately.

High aerodynamic heating is generally associated with high speed flight at high altitudes with correspondingly low ambient pressure. Pressure increases rapidly to one atmosphere as the vehicle slows and descends for landing. For an adiabatic structure, the maximum temperature may occur long after the heating pulse is completed. Therefore, a simplified pressure history was investigated. The pressure was assumed to have a uniform value, P_1, during the heating pulse and a different uniform value, P_2, after the heating pulse. The one-dimensional finite element model was used to investigate the effect of this simplified pressure profile on the calculated maximum structural temperature. Again, the material property values and heating parameters were the same as those used for the baseline results in Table 3, except

Table 5. Effect of temperature dependent insulator specific heat capacity

Insulator Temperature	Finite Element T, K	$c_{pe}(T)$ $\left(\frac{J}{kgK}\right)$	γ	τ_h	T_{ma}(Series) K	T_{ma}(Eq. 20) K
T_i	288.71	688.0	0.9393	0.22191	426.96	428.13
T_{ma}	**418.44**	909.6	1.2419	0.16784	**414.04**	**409.87**
$\frac{T_{ha}+T_i}{2}$	827.59	1209.8	1.6518	0.12620	400.15	393.55
		$t_h =$ **1500s, T_{ha} =1366K**				
T_i	288.71	688.0	0.9393	0.11095	358.66	357.39
T_{ma}	**350.88**	800.4	1.0929	0.09537	**355.88**	**352.19**
$\frac{T_{ha}+T_i}{2}$	827.59	1209.8	1.6518	0.06310	344.74	339.88
		$t_h =$ **750s, T_{ha} =1366K**				
T_i	288.71	688.0	0.9393	0.44382	554.38	561.19
T_{ma}	**531.14**	1052.3	1.4368	0.29016	**518.86**	**511.89**
$\frac{T_{ha}+T_i}{2}$	827.59	1209.8	1.6518	0.25239	506.19	497.47
		$t_h =$**3000s, T_{ha} =1366K**				
T_i	288.71	688.0	0.9393	0.22191	357.84	358.42
T_{ma}	**355.42**	808.7	1.1041	0.18879	**354.16**	**352.99**
$\frac{T_{ha}+T_i}{2}$	558.15	1072.3	1.4640	0.14238	347.37	344.45
		$t_h =$**1500s, T_{ha} =828K**				

that the constant value of k_e was replaced by the temperature and pressure dependent values from Table B3. The values of P_1 and P_2 were systematically varied between values of 0.0001, 0.001, 0.01, 0.1, and 1.0 atm. The resulting structural temperature histories are shown in Fig. 13. Different color lines represent different values of P_1. Different line patterns represent different values of P_2: solid is 1.0 atm, dashed is 0.1 atm, and dotted is 0.01 atm. The curves in Fig. 13 exhibit a consistent pattern. The maximum structural temperature depends only on P_1. Different values of P_2, cause the time of maximum temperature to vary, but the maximum temperature itself varies less than 0.2K over this wide range of P_2 values. Similar results were obtained for Saffil insulation in air.

Thermal conductivity of the insulator is also generally a strong function of temperature. A simple approach for choosing an effective constant value of k_e would be to use the conductivity for a pressure, P_1, at a temperature, T_{ke}, that is the average of T_{ha} and T_i. A slightly more general approach would be to choose a thermal conductivity at a temperature defined by

$$T_{ke} = T_i + f_{ke}T_h \qquad (25)$$

where f_{ke} is the fraction (0 to 1) of the insulator temperature range. A value of 0.5 would result in a simple average of T_{ha} and T_i.

A parametric numerical study was performed to determine if there was a sin-
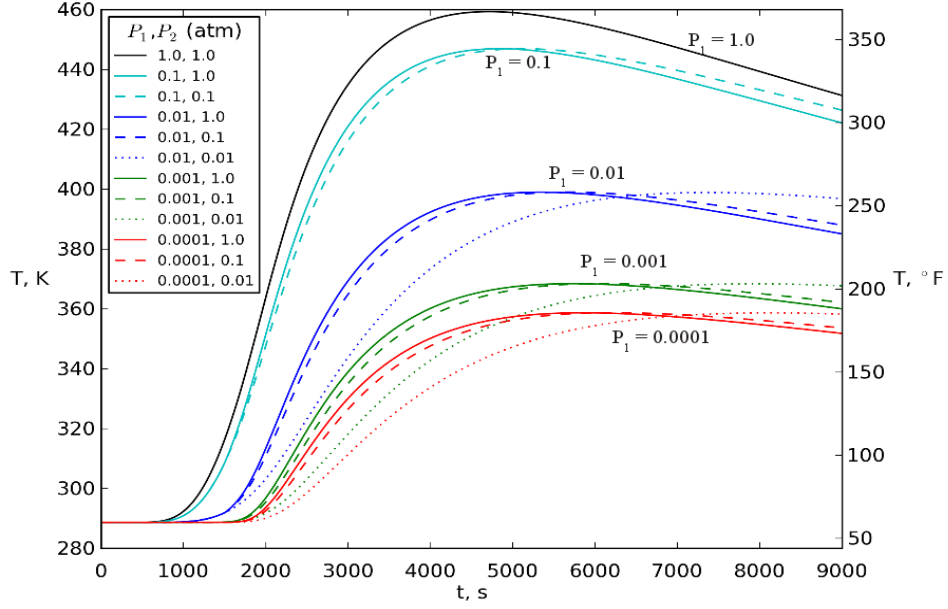
Figure 13. Structural temperature histories for different ambient pressures

gle value of f_{ke} that could be used to predict accurately the maximum structural temperature. Results for LI-900 are shown in Table 6, and for Saffil insulation in Table 7. A range of parameters were varied, including P_1, T_h, t_h, d_e, and ρ_e. All other material properties, except k_e, were held constant. In Table 7 the default value of d_e is 3 in. (0.0762 m) and the default value of ρ_e is 4.5 $\frac{lbm}{ft^3}$ (72 $\frac{kg}{m^3}$). For each combination of parameters, the one-dimensional finite element model, with $k_e(P_1, T)$, was used to calculate the maximum structural temperature (column 2 of Tables 6 and 7). The series solution, Eqs. 16 and 19, was solved iteratively to find the fixed value of k_e that would produce the same maximum structural temperature as the finite element solution. The associated values of T_{ke} (column 3 of Tables 6 and 7) and f_{ke} (column 4 of Tables 6 and 7) were also calculated. For the majority of the results shown, f_{ke} ranged between 0.57 and 0.62. A value of 0.60 was chosen for f_{ke}, and the corresponding values of T_{ke}, $k_e(P_1, T_{ke})$, and τ_h (column 5 of Tables 6 and 7) were calculated. The resulting approximate maximum structural temperatures were calculated using the series solution (column 6 of Tables 6 and 7) and the approximate solution (column 7 of Tables 6 and 7). For $f_{ke} = 0.6$, Tables 6 and 7 show good agreement between the finite element and series solutions for maximum structural temperature. Over most of the parameter ranges the approximate solution is close to the series solution, but starts to diverge for small values of γ (Table 7), as expected from the errors shown in Figs. 9 and 10.

Table 6. Maximum structural temperature calculated using effective LI-900 thermal conductivity

P_1 atm	Finite Element T_{ma}, K	T_{ke} K	f_{ke}	τ_h	T_{ma}(Series) K	T_{ma}(Eq. 20) K
0.0001	358.72	954.0	0.617	0.07525	356.48	351.14
0.001	368.45	955.9	0.619	0.08577	365.86	360.21
0.01	399.02	950.6	0.614	0.12071	396.79	390.27
0.1	446.95	936.5	0.601	0.17853	447.03	439.33
$\gamma = \mathbf{1.6903}$, $t_h = \mathbf{1500s}$, $T_{ha} = \mathbf{1367K}$				$f_{ke} = \mathbf{0.6}$, $T_{ke} = \mathbf{935.6K}$		
0.0001	422.26	1142.1	0.629	0.10789	410.38	402.56
0.001	429.54	1126.7	0.618	0.11867	422.34	414.20
0.01	469.68	1116.0	0.610	0.15824	465.80	456.62
0.1	541.09	1117.0	0.611	0.22374	535.89	525.19
$\gamma = \mathbf{1.6903}$, $t_h = \mathbf{1500s}$, $T_{ha} = \mathbf{1644K}$				$f_{ke} = \mathbf{0.6}$, $T_{ke} = \mathbf{1102.2K}$		
0.0001	323.89	756.6	0.585	0.05398	324.93	321.53
0.001	330.85	756.9	0.585	0.06443	331.88	328.19
0.01	351.52	779.1	0.613	0.09315	350.89	346.55
0.1	381.23	756.1	0.584	0.14216	382.93	377.75
$\gamma = \mathbf{1.6903}$, $t_h = \mathbf{1500s}$, $T_{ha} = \mathbf{1089K}$				$f_{ke} = \mathbf{0.6}$, $T_{ke} = \mathbf{768.9K}$		
0.0001	304.69	592.2	0.581	0.03755	305.27	303.42
0.001	309.04	587.3	0.571	0.04795	309.80	307.70
0.01	321.12	599.3	0.583	0.07527	321.65	319.06
0.1	336.38	591.6	0.580	0.11168	337.31	334.26
$\gamma = \mathbf{1.6903}$, $t_h = \mathbf{1500s}$, $T_{ha} = \mathbf{811K}$				$f_{ke} = \mathbf{0.6}$, $T_{ke} = \mathbf{602.3K}$		
0.0001	293.96	439.2	0.615	0.02550	294.10	293.40
0.001	295.79	438.8	0.613	0.03445	295.93	295.10
0.01	301.10	442.2	0.627	0.06018	301.16	300.07
0.1	306.23	440.0	0.618	0.08544	306.28	305.00
$\gamma = \mathbf{1.6903}$, $t_h = \mathbf{1500s}$, $T_{ha} = \mathbf{533K}$				$f_{ke} = \mathbf{0.6}$, $T_{ke} = \mathbf{435.6K}$		
0.0001	335.18	951.5	0.615	0.05017	334.03	329.61
0.001	341.67	953.2	0.616	0.05718	340.32	335.61
0.01	361.98	945.1	0.609	0.08047	361.14	355.64
0.1	393.83	926.2	0.591	0.11902	395.30	388.82
$\gamma = \mathbf{1.6903}$, $t_h = \mathbf{1000s}$, $T_{ha} = \mathbf{1367K}$				$f_{ke} = \mathbf{0.6}$, $T_{ke} = \mathbf{935.6K}$		
0.0001	382.33	956.2	0.619	0.10034	378.80	372.77
0.001	395.35	958.9	0.622	0.11436	391.19	384.82
0.01	436.15	955.6	0.619	0.16095	431.90	424.54
0.1	499.87	947.6	0.611	0.23804	497.16	488.41
$\gamma = \mathbf{1.6903}$, $t_h = \mathbf{2000s}$, $T_{ha} = \mathbf{1367K}$				$f_{ke} = \mathbf{0.6}$, $T_{ke} = \mathbf{935.6K}$		

Table 7. Maximum structural temperature calculated using effective Saffil thermal conductivity ($t_h = 1500$s)

P_1 atm	Finite Element T_{ma}, K	T_{ke} K	f_{ke}	τ_h	T_{ma}(Series) T_{ma}, K	T_{ma}(Eq. 20) T_{ma}, K
0.0001	385.23	931.5	0.596	0.16694	386.50	387.99
0.001	405.99	941.7	0.606	0.19850	404.57	407.07
0.01	457.55	935.0	0.599	0.29376	457.92	463.63
0.1	482.63	932.8	0.597	0.34120	483.89	491.02
$\rho_e = 72 \frac{kg}{m^3}$, $d_e = 0.0762$m, $\gamma = 0.8452$, $T_{ha} =$1367K				$f_{ke} = 0.6$, $T_{ke} = 935.6$K		
0.0001	329.76	745.7	0.571	0.10155	333.20	332.72
0.001	344.56	754.8	0.582	0.13288	346.74	347.07
0.01	379.25	753.7	0.581	0.21580	382.05	384.33
0.1	393.60	752.7	0.580	0.25156	396.98	400.16
$\rho_e = 72 \frac{kg}{m^3}$, $d_e = 0.0762$m, $\gamma = 0.8452$, $T_{ha} =$1089K				$f_{ke} = 0.6$, $T_{ke} = 768.9$K		
0.0001	313.96	588.3	0.573	0.12546	315.57	317.88
0.001	328.84	592.0	0.581	0.19465	330.10	334.55
0.01	359.31	587.4	0.572	0.34894	361.62	371.04
0.1	370.14	587.8	0.572	0.40521	372.71	383.95
$\rho_e = 72 \frac{kg}{m^3}$, $d_e = 0.0508$m, $\gamma = 0.5634$ $T_{ha} =$811K				$f_{ke} = 0.6$, $T_{ke} = 602.2$K		
0.0001	301.90	425.9	0.561	0.24284	302.68	307.68
0.001	316.59	428.9	0.573	0.50759	317.22	328.42
0.01	339.90	430.0	0.577	0.96849	340.69	361.57
0.1	346.37	431.3	0.582	1.10387	347.12	370.46
$\rho_e = 72 \frac{kg}{m^3}$, $d_e = 0.0254$m, $\gamma = 0.2817$, $T_{ha} =$533K				$f_{ke} = 0.6$, $T_{ke} = 435.6$K		
0.0001	358.43	756.42	0.584	0.22445	361.50	369.79
0.001	379.61	763.0	0.593	0.28701	381.81	392.56
0.01	416.06	760.1	0.589	0.40934	418.58	435.96
0.1	427.75	760.5	0.590	0.44890	430.34	449.61
$\rho_e = 48 \frac{kg}{m^3}$, $d_e = 0.0762$m, $\gamma = 0.5634$, $T_{ha} =$1089K				$f_{ke} = 0.6$, $T_{ke} = 768.9$K		

6.4 Heating History Profile

For hypersonic aerospace vehicles, surface heating histories can vary greatly with the vehicle mission, trajectory, configuration, and location on the vehicle. Surface heating histories are often provided to a TPS designer in the form of radiation equilibrium heating rates, radiation equilibrium temperatures, convective heating coefficients with total enthalpies or recovery temperatures, or a series of heating rates at constant wall temperatures that bracket the expected surface temperature range. For simplicity, the current study will only consider radiation equilibrium temperature histories, which are suitable for well insulated surfaces that have relatively low thermal mass at the surface. Radiation equilibrium temperature histories can also be readily calculated from the other forms of heating histories.
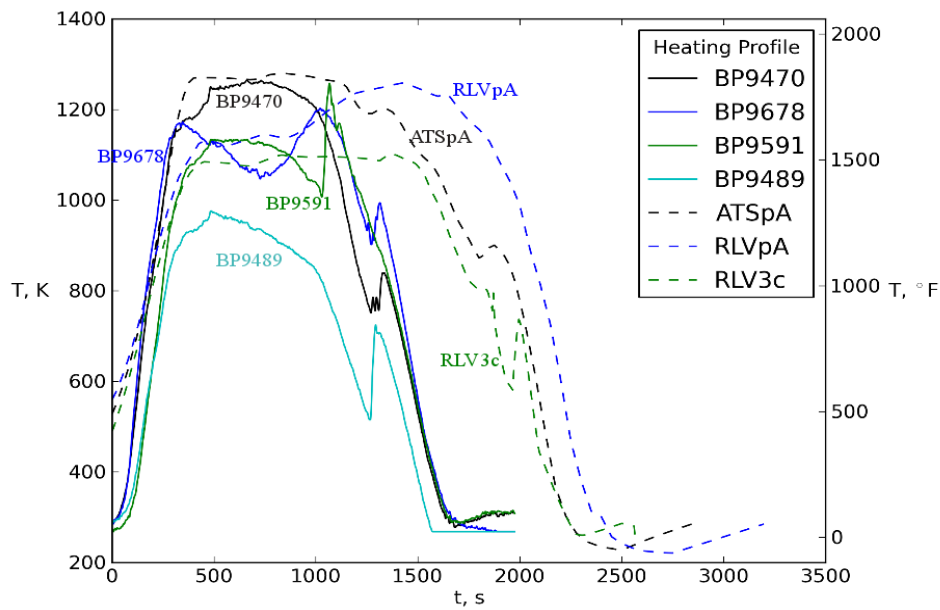

Figure 14. Surface temperature histories

For the current study, surface temperature histories were chosen from Space Shuttle Orbiter entry flight data [8, 9] and from previous studies [10, 11] of single stage-to-orbit reusable launch vehicles (RLV's). A total of seven surface temperature histories are shown in Fig. 14. Surface temperature histories from four different body points (BP9740, BP9678, BP9591, and BP9489) during the same atmospheric entry flight of the Shuttle Orbiter were chosen to illustrate a range of different profile shapes. The flight temperature data was smoothed to reduce noise from the crude discretization produced by the flight instrumentation. Two heating histories from an earlier TPS parametric weight study [10], body point A on the windward center line of a winged cylindrical vehicle for the Access to Space study (ATSpA), and body point A on windward centerline of a lifting body reusable launch vehicle (RLVpA) are also shown in Fig. 14. The seventh surface temperature history, also studied in
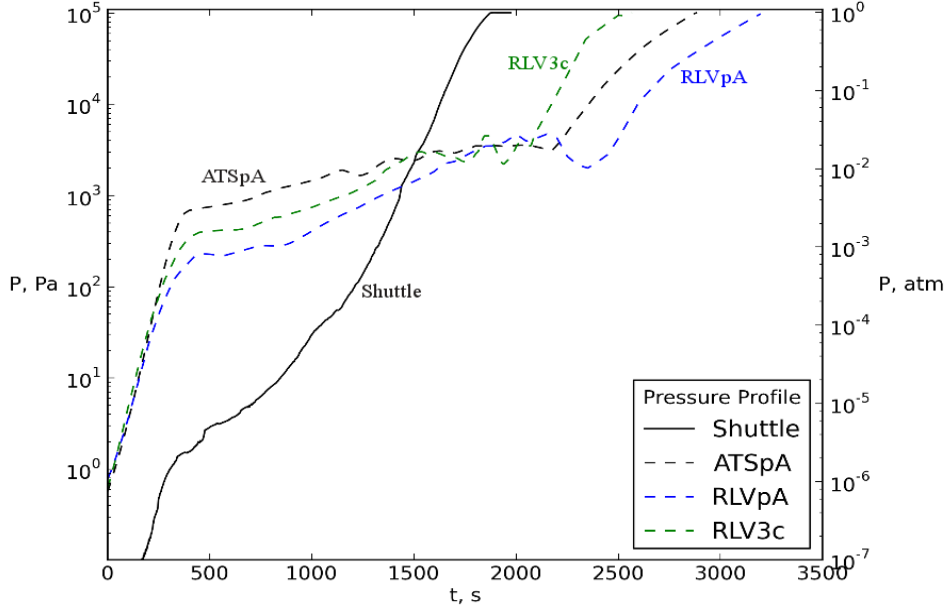
25

Figure 15. Ambient pressure histories

Reference [11], was for a point on the windward center line of a slightly different variation of the lifting body vehicle (RLV3c). The corresponding ambient pressure histories are shown in Fig. 15.

The challenge was to find an equivalent square heating pulse for each of the heating histories that would enable the analytical solution to calculate an accurate estimate of the maximum structural temperature. The first step in idealizing the heating histories was to simplify the temperature histories in Fig. 14 by truncating the variable low temperature portions of each history at the beginning and end. The histories were truncated by eliminating any portions below a threshold surface temperature defined by

$$T_{thr} = T_i + f_{thr}(T_{mx} - T_i) \tag{26}$$

where T_{mx} is the maximum surface temperature for a surface temperature history, and f_{thr} is a fraction of the surface temperature range.

Several quantities, including integrated heat load, integrated absolute surface temperature, and integrated surface temperature rise from the initial temperature, were integrated over the time of the truncated temperature histories.

The one-dimensional finite element model with fixed material properties from Table 1 was used to calculate the maximum structural temperature for a structural thickness of 0.125 inch and insulator thicknesses of 1, 2, 3, and 4 inches for each heating history. The resulting maximum structural temperatures were plotted as a function of various integral values, such as integrated heat load, integrated absolute temperature, and integrated surface temperature rise, in hopes of identifying a clear correlation. A linear correlation, Fig. 16, was discovered between the maximum

26

structural temperature rise, T_m, and the integrated surface temperature rise from the initial temperature, which is defined as

$$I_T = \int_{t_1}^{t_2} (T - T_i)dt \qquad (27)$$

where t_1 and t_2 are the beginning and ending times of the truncated temperature history.
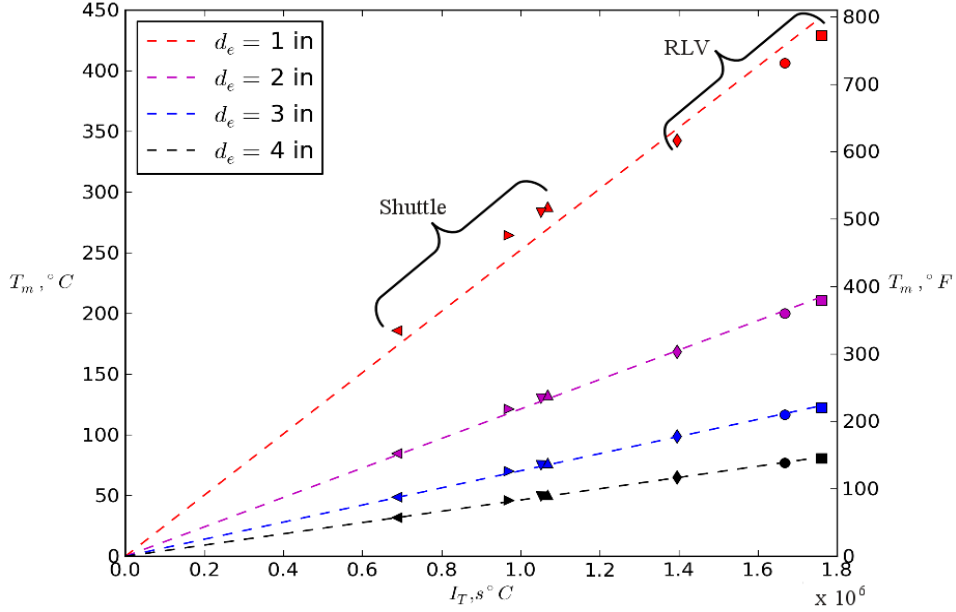

Figure 16. Maximum structural temperature vs integrated surface temperature rise

In Fig. 16, the maximum structural temperature rise is shown as a function of the integral defined in Eq. 27. Each marker shape represents one of the seven surface heating histories from Fig. 14. The triangular symbols represent the four shuttle histories and the other symbols represent the RLV histories. The dashed lines represent the best fit line for all the maximum structural temperatures calculated using the finite element model at each insulator thickness. The lines were constrained to pass through the origin. The figure implies that for each configuration with fixed material properties, the maximum structural temperature rise is directly proportional to the integral defined in Eq. 27. For the simple square heat pulse, that integral is simply

$$I_T = T_h t_h \qquad (28)$$

To determine a reasonable equivalent square heat pulse it is helpful to bound the ranges of the two parameters that define it. The maximum possible value of t_h would be the time span of the truncated surface temperature history, $t_2 - t_1$, and the largest that T_h could be is the maximum surface temperature rise, $T_{mx} - T_i$. Therefore,

the smallest that t_h could be is $I_T/(T_{mx} - T_i)$. For fixed material properties, the series solution was used to calculate T_m by varying combinations of t_h and T_h for fixed values of I_T. The calculated value of T_m was almost totally a function of I_T and showed little sensitivity to the particular combinations of t_h and T_h over their feasible ranges. However, for variable material properties, it is important to chose a combination of t_h and T_h that will enable calculation of constant effective properties and average pressure during the heating pulse, P_1. A simple approach is to use an average of the bounding values of t_h.

$$t_h = \frac{(t_2 - t_1) + \frac{I_T}{T_{mx} - T_i}}{2} \tag{29}$$

Then T_h can be readily found from Eq. 28. The resulting square heat pulse can then be centered in the truncated time range between t_1 and t_2 for the purposes of calculating an average value of P_1, P_{avg}.
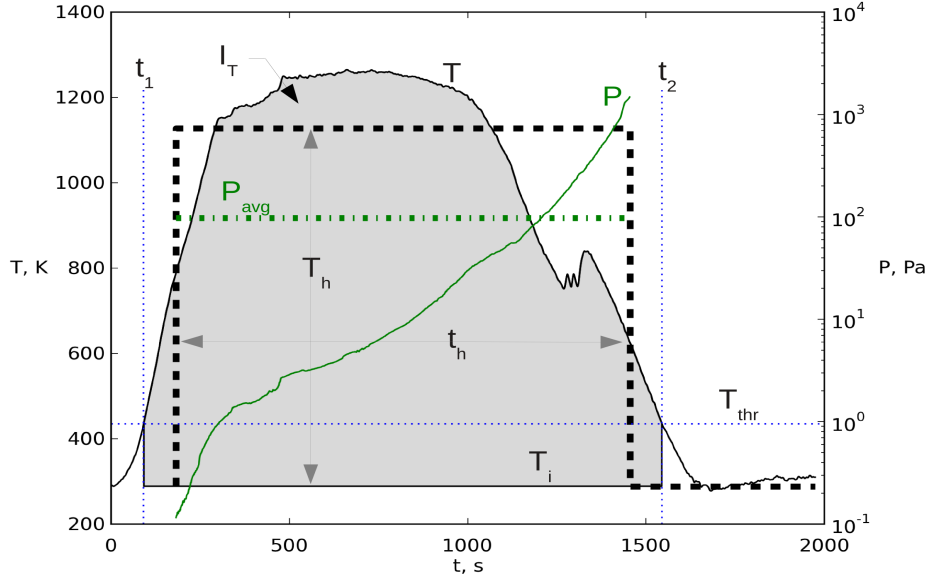
Figure 17. Simplified heating and pressure histories for BP9740

This approach for simplifying the surface heating history of Shuttle Orbiter body point 9740 is illustrated in Fig. 17. The solid black line represents the surface temperature history for BP9470. The horizontal blue dotted line represents the threshold temperature defined in Eq. 26 for $f_{thr} = 0.15$. The vertical blue dotted lines, t_1 and t_2, bound the truncated heating pulse. The shaded area illustrates the integral defined by Eq. 27. The heavy black dashed line represents the equivalent square heating pulse with t_h calculated from Eq. 29. The square heat pulse has been centered between t_1 and t_2 for the purpose of calculating an average pressure to use as P_1. The ambient pressure over the duration of the square heat pulse is indicated

by a solid green line. The heavy green dot-dash line represents a simple average of the pressure over the interval of the square heat pulse.

Selecting the threshold temperature, or more specifically f_{thr}, for truncating the surface temperature histories is not straightforward. The intent of truncating the temperature histories is to capture the main heating pulse without any spurious complications from variations in convective cooling effects before landing or the missing initial portion of the heating history (RLV histories). The heating history simplifications illustrated in Fig. 17 were applied to all seven heating histories for three different values of f_{thr}: 0.10, 0.15, and 0.20. Table 8 lists the resulting calculated quantities. The second column shows the maximum surface temperature rise. The third column shows the threshold temperature for the given value of f_{thr} and the fourth and fifth columns show the times bounding the truncated heating interval. Columns 6 and 8 show the maximum and minimum possible durations for the equivalent square heat pulse and column 9 is their average. The last three columns contain the values that would be used for further calculations using the analytical solution. The integral in column 7 changes little over this range of f_{thr}, which indicates that there should be little effect on the calculated maximum structural temperature for fixed material properties.

Table 8. Simplified surface temperature histories

Profile	$T_{mx} - T_i$	T_{thr}	t_1	t_2	$t_2 - t_1$	I_T	$\frac{I_T}{T_{mx}-T_i}$	t_h	T_h	P_{avg}
	$°C$	K	s	s	s	$10^3 s\ °C$	s	s	$°C$	Pa
				$f_{thr} = 0.10$						
BP9470	976.4	386.3	77.2	1575.0	1497.8	1073.5	1099.4	1298.6	826.6	122.7
BP9678	914.0	380.1	76.7	1593.8	1517.1	1055.4	1154.7	1335.9	790.0	163.3
BP9591	969.3	385.6	126.4	1583.4	1457.0	975.5	1006.4	1231.7	792.0	122.2
BP9489	687.5	357.5	99.3	1516.8	1417.5	689.0	1002.1	1209.8	569.5	64.7
ATSpA	990.9	387.8	0.0	2166.3	2166.3	1670.4	1685.7	1926.0	867.3	1756.6
RLVpA	969.9	385.7	0.0	2297.9	2297.9	1763.4	1818.0	2058.0	856.9	1025.5
RLV3c	814.1	370.1	0.0	2160.2	2160.2	1399.1	1718.5	1939.4	721.4	1401.4
				$f_{thr} = 0.15$						
BP9470	976.4	435.2	91.4	1544.7	1453.3	1068.1	1093.9	1273.6	838.6	98.0
BP9678	914.0	425.8	88.1	1565.9	1477.8	1051.0	1149.8	1313.8	799.9	133.0
BP9591	969.3	434.1	141.7	1554.2	1412.5	970.1	1000.8	1206.6	804.0	99.7
BP9489	687.5	391.8	114.2	1498.6	1384.3	686.1	998.0	1191.2	576.0	59.1
ATSpA	990.9	437.3	0.0	2145.7	2145.7	1667.8	1683.1	1914.4	871.2	1756.6
RLVpA	969.9	434.2	0.0	2269.7	2269.7	1760.0	1814.5	2042.1	861.8	1025.5
RLV3c	814.1	410.8	0.0	2125.1	2125.1	1395.5	1714.2	1919.6	727.0	1364.6
				$f_{thr} = 0.20$						
BP9470	976.4	484.0	103.5	1523.2	1419.6	1062.3	1088.0	1253.8	847.3	84.0
BP9678	914.0	471.5	95.7	1538.6	1442.9	1045.4	1143.7	1293.3	808.3	107.3
BP9591	969.3	482.6	154.5	1529.6	1375.1	963.7	994.2	1184.7	813.5	82.7
BP9489	687.5	426.2	127.9	1480.9	1353.0	682.4	992.6	1172.8	581.9	54.2
ATSpA	990.9	486.9	0.0	2125.2	2125.2	1664.2	1679.5	1902.4	874.8	1732.7
RLVpA	969.9	482.7	0.0	2244.6	2244.6	1755.8	1810.2	2027.4	866.0	974.2
RLV3c	814.1	451.5	0.0	2091.9	2091.9	1390.8	1708.4	1900.2	732.0	1331.4
1	2	3	4	5	6	7	8	9	10	11

The equivalent square heat pulses, defined by the values of t_h and T_h in Table 8, and the fixed material properties from Table 1 were substituted into the series

solution to calculate the maximum structural temperature rise. The temperature was predicted for a structural thickness of 0.125 in. and insulator thicknesses of 1, 2, 3, and 4 in. for each equivalent square heat pulse and compared to the finite element results shown in Fig. 16. The largest errors in maximum structural temperature rise were -5.4%, -5.9%, and -6.5% for f_{thr} values of 0.10, 0.15, and 0.20 respectively. Therefore, for fixed material properties, the solution is not sensitive to the threshold temperature over the range considered. However, variable material properties are sensitive to both T_h and P_{avg}, which vary somewhat with f_{thr}, as shown in Table 8. With these considerations in mind, a value of $f_{thr} = 0.15$ was chosen for further calculations.

6.5 Approximation of Realistic Simulations

The key remaining question is: how accurately can the analytical solution, with the previously described effective material properties and simplified square heat pulse, predict the maximum structural temperature calculated using a finite element solution with variable material properties and a time-accurate surface temperature history? The one-dimensional finite element model with temperature-dependent structural properties from Table B1 and insulator properties from Tables B2 and B3 was used to calculate the maximum structural temperature for a structural thickness of 0.125 in. and LI-900 insulator thicknesses of 1, 2, 3, and 4 in. for each heating history.

For comparison, the maximum structural temperature was calculated for each surface temperature history and geometry using the series and approximate analytical solutions, with the following approximations.

$$c_{ps} = c_{ps}(T_{cs}), \text{ where } T_{cs} = T_i + \frac{T_m}{2}, \tag{30}$$

$$c_{pe} = c_{pe}(T_{ce}), \text{ where } T_{ce} = T_i + T_m, \text{ and} \tag{31}$$

$$k_e = k_e(T_{ke}, P_{avg}), \text{ where } T_{ke} \text{ is defined in Eq. 25} \tag{32}$$

Values for t_h, T_h, and P_{avg} are taken from Table 8 for $f_{thr} = 0.15$.

One difficulty is that the maximum structural temperature rise, T_m, must be known to calculate the effective constant properties. This difficulty can be readily overcome by making an initial guess and iterating to a converged solution. The series solution and both approximate analytical solutions, Eqs. 20 and 21 were each iterated independently to arrive at their respective converged solutions.

The finite element and analytical solutions for maximum structural temperature are compared in Fig. 18. The figure shows the maximum structural temperature rise as a function of LI-900 tile thickness. The solid circles represent the finite element solutions, the solid lines represent the series solution, the dashed lines represent the approximate solution given by Eq. 20, and the dotted lines represent the approximate solution given by Eq. 21. The colors correspond to the applied surface temperature histories: black - Shuttle orbiter body point 9470, green - Shuttle
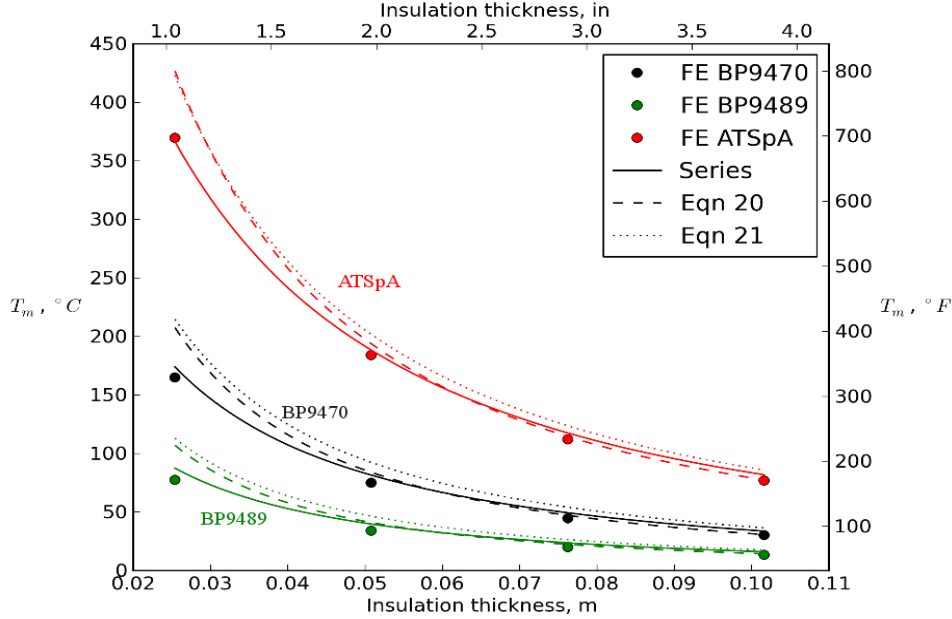
Figure 18. Maximum structural temperature rise vs insulation thickness

orbiter body point 9489, and red - ATS reusable launch vehicle point A (windward centerline). The series solution agrees with the finite element solution to within -0.9% and 18.7% for the predicted maximum structural temperature rise of the cases shown on Fig. 18. The close agreement between the finite element results and the series solution tends to validate the methodology used to calculate the effective material properties and to map the transient surface temperature history to an equivalent square pulse. The two approximate equations track the series solution and the finite element solution well for most of the LI-900 thickness range, but start to diverge for small thickness values.

Table 9 gives the detailed numerical comparisons between the finite element calculations and results using the equations developed in this paper. The table is divided into seven sections with each section consisting of results for four different insulator thicknesses for a surface temperature history identified in bold print. For each insulation thickness, values of the two governing nondimensional parameters (associated with the series solution) are given, based on the effective constant material properties and equivalent square heating pulse defined previously. The finite element prediction of the maximum structural temperature rise is given for variable material properties and a time-accurate surface heating history. The series and approximate solutions for the maximum structural temperature rise are also shown, along with their errors relative to the finite element solution. The best assessment of the accuracy of using the material property simplifications combined with the surface temperature history simplifications is error associated with the series solution. The approximate solution has the same errors as the series solution combined with the approximation errors illustrated in Fig. 10. The errors for the series so-

31

lution range from 5.6% to 21.3%. The series solution is remarkably close to the finite element solution, considering the complexity of the numerical simulation and the large variation of material properties that occurs with time. For the much simpler approximate equations, Eq. 20 has errors that range from 1.5% to 38.2% and Eq. 21 has errors that range from 9.6% to 46.0%. The errors for the approximate solutions start to get large for relatively small values of γ, as expected from the errors shown in Fig. 10. The series solution errors for the reusable launch vehicles (ATSpA, RLVpA, and RLV3c) are less than 10% for all calculated cases.

7 Mass of Insulated Structure

For aerospace vehicles reducing mass is of utmost importance. Therefore, it is helpful to develop further insight into the interplay between the mass of structure and the mass of insulator required to limit the structural temperature. The mass per unit area of this simplified, insulated structure can be written simply as

$$m = m_e + m_s = \rho_e d_e + \rho_s d_s \tag{33}$$

The relationship between d_e and d_s that is required to limit the maximum structural temperature to a specified value is given by Eq. 21. By substituting Eqs. 4 and 10 into Eq. 21 and rearranging terms, the following expression can be obtained.

$$d_s d_e^3 = \frac{(k_e t_h)^2}{2(\rho_s c_{ps})(\rho_e c_{pe})\left(-ln(1 - \frac{T_m}{T_h})\right)^2} \tag{34}$$

The equation can be further manipulated to give an explicit expression for d_e. This provides a useful equation to calculate the insulator thickness required to limit the maximum structural temperature to a specified value.

$$d_e = \left(\frac{(k_e t_h)^2}{2(\rho_s c_{ps} d_s)(\rho_e c_{pe})\left(-ln(1 - \frac{T_m}{T_h})\right)^2}\right)^{\frac{1}{3}} \tag{35}$$

Substituting Eq. 35 into Eq. 33 produces an expression for mass per unit area as a function of structural thickness.

$$m = \left(\frac{\left(\frac{\rho_e k_e}{\sqrt{c_{pe}}}\right)^2 t_h^2}{2\rho_s d_s c_{ps}\left(-ln(1 - \frac{T_m}{T_h})\right)^2}\right)^{\frac{1}{3}} + \rho_s d_s \tag{36}$$

The first term in Eq. 36 represents the mass of insulator required to limit the structure to the specified maximum temperature and the second term represents structural mass. Eq. 36 can be written as a function of m_s.

Table 9. Maximum structural temperature rise for LI900 insulation

d_e	γ	τ_h	FE	Series	error	Eq. 20	error	Eq. 21	error
m			$^\circ C$	$^\circ C$	%	$^\circ C$	%	$^\circ C$	%
BP9470									
0.0254	0.4367	0.6536	164.86	174.10	5.6	207.58	25.9	214.64	30.2
0.0508	0.7858	0.1889	74.84	81.58	9.0	83.99	12.2	92.40	23.5
0.0762	1.1128	0.0902	44.74	49.42	10.5	47.22	5.5	54.23	21.2
0.1016	1.4400	0.0527	30.33	33.74	11.2	30.79	1.5	36.51	20.4
BP9678									
0.0254	0.4364	0.6857	152.83	173.38	13.4	206.89	35.4	213.33	39.6
0.0508	0.7857	0.1980	68.76	81.49	18.5	84.03	22.2	92.15	34.0
0.0762	1.1128	0.0946	41.05	49.40	20.3	47.30	15.2	54.14	31.9
0.1016	1.4400	0.0552	27.81	33.73	21.3	30.85	10.9	36.47	31.1
BP9591									
0.0254	0.4288	0.6144	139.86	155.54	11.2	186.49	33.3	193.71	38.5
0.0508	0.7735	0.1767	63.32	72.47	14.4	74.65	17.9	82.61	30.5
0.0762	1.1010	0.0839	37.78	43.76	15.8	41.70	10.4	48.20	27.6
0.1016	1.4290	0.0488	25.58	29.83	16.6	27.10	5.9	32.35	26.5
BP9489									
0.0254	0.3969	0.5056	77.47	87.58	13.0	107.09	38.2	113.09	46.0
0.0508	0.7285	0.1408	33.92	39.79	17.3	41.10	21.2	46.49	37.1
0.0762	1.0588	0.0651	20.08	23.75	18.3	22.41	11.6	26.52	32.1
0.1016	1.3900	0.0373	13.55	16.09	18.7	14.39	6.1	17.60	29.8
ATSpA									
0.0254	0.4826	1.3822	369.70	366.53	-0.9	426.90	15.5	423.03	14.4
0.0508	0.8856	0.4003	184.05	188.32	2.3	193.76	5.3	201.79	9.6
0.0762	1.2413	0.1957	112.23	117.62	4.8	114.58	2.1	123.82	10.3
0.1016	1.5723	0.1178	76.97	81.86	6.3	77.45	0.6	85.93	11.6
RLVpA									
0.0254	0.4803	1.3174	358.76	348.28	-2.9	405.92	13.1	403.15	12.4
0.0508	0.8764	0.3826	175.04	177.50	1.4	182.78	4.4	190.99	9.1
0.0762	1.2327	0.1863	106.19	110.50	4.1	107.55	1.3	116.67	9.9
0.1016	1.5589	0.1122	72.75	76.85	5.6	72.59	-0.2	80.88	11.2
RLV3c									
0.0254	0.4710	1.2408	270.03	276.63	2.4	324.47	20.2	323.31	19.7
0.0508	0.8446	0.3626	131.45	139.07	5.8	143.92	9.5	151.17	15.0
0.0762	1.1880	0.1760	79.73	86.22	8.1	84.07	5.4	91.61	14.9
0.1016	1.5121	0.1050	54.48	59.67	9.5	56.23	3.2	63.12	15.9

$$m = \left(\frac{\left(\frac{\rho_e k_e}{\sqrt{c_{pe}}}\right)^2 t_h^2}{2c_{ps}\left(-ln(1-\frac{T_m}{T_h})\right)^2} \right)^{\frac{1}{3}} m_s^{-\frac{1}{3}} + m_s \qquad (37)$$

7.1 Material Properties and Insulator Mass

The first term in Eq. 37 represents the mass of insulator required to limit the structure to the specified maximum temperature. Inspection of this equation illustrates the effect of key parameters on required insulator mass.

$$m_e = \left(\frac{\left(\frac{\rho_e k_e}{\sqrt{c_{pe}}}\right)^2}{c_{ps}\left(-ln(1-\frac{T_m}{T_h})\right)^2} \right)^{\frac{1}{3}} \left(\frac{t_h^2}{2m_s} \right)^{\frac{1}{3}} \qquad (38)$$

From Eq. 38, it is obvious that a longer heat pulse (increased t_h) will result in a larger required insulator mass. Similarly, a larger structural mass will provide more structural heat sink capacity and require less insulator mass. For a given structural mass and a particular transient heating pulse, required insulation mass will be determined by the thermal properties of the insulator and structure.

The specific heat capacities of insulators and structural materials vary significantly with temperature and the thermal conductivity of low density insulators is a function of both temperature and pressure. Therefore, it is not immediately obvious which material property values to use in the preceding equations to obtain results that are meaningful and useful. However, the previously derived expressions for equivalent constant thermal properties, Eqs. 30, 31, and 32, can be used to calculate values of c_{ps}, c_{pe}, and k_e for each surface temperature history. The quantities defining the equivalent square heating pulses, t_h, T_h and P_{avg}, are listed in Table 8 for the seven heating histories previously studied. The first four temperature histories were measured at four different locations on the windward surface of a Shuttle Orbiter during a single atmospheric entry flight [8,9]. It is interesting to note the variation in the equivalent square heating pulses that occur over just the windward surface in a single flight. The last three heating histories were predicted for a single point on the windward surface of three different proposed reusable launch vehicles [10,11].

Inspection of Eqs. 37 and 38 reveals that the thermal properties of the structure and insulator can each be grouped separately. These grouped properties have the potential to be useful for comparing the thermal effectiveness of both the structural and insulator materials.

The specific heat capacity and maximum allowable temperature of the structure directly affect the required insulation mass. However, the thermal properties of the structure are coupled to the amplitude of the equivalent square heating pulse, T_h. The following expression is a candidate figure of merit for the thermal effectiveness of the structural material.

$$\beta_s = c_{ps} \left(-ln(1 - \frac{T_m}{T_h}) \right)^2 \tag{39}$$

A larger value of this parameter will lead to a smaller required mass of insulation. Therefore a structure with a high specific heat capacity and high maximum temperature limit will tend to require less insulation.

For steady state heat conduction, minimizing the product of insulator density and thermal conductivity, $\rho_e k_e$, minimizes the mass of required insulator [11]. However, a similar figure of merit for minimum mass of insulation subjected to transient heating has not been available. The grouping of insulator properties in Eq. 38 suggests a candidate figure of merit for minimum mass insulation for a transient heating pulse (or at least for the simplified heat pulse in this derivation).

$$\kappa_e = \frac{\rho_e k_e}{\sqrt{c_{pe}}} \tag{40}$$

A smaller value of this parameter will lead to a smaller required mass of insulation. Therefore, a low mass insulator for the transient heat pulse should have a combination of low $\rho_e k_e$ and high c_{pe}.

7.2 Minimum Mass of Insulated Structure

The mass of the insulated structure, calculated using Eq. 37, is obviously a function of the mass of the structural material. Increasing the amount of structural mass linearly adds to the total mass, but results in a corresponding decrease in the mass of required insulation. Therefore, in the absence of any overriding structural requirements, there should be a structural mass for which the total mass is minimum. The structural mass for which the total mass is minimum can be readily calculated by taking the first derivative of Eq. 37 with respect to m_s and setting it equal to zero. The result can be solved for m_s to produce

$$m_{so} = 54^{(-\frac{1}{4})} \sqrt{t_h} \left(\frac{\left(\frac{\rho_e k_e}{\sqrt{c_{pe}}} \right)^2}{c_{ps} \left(-ln \left(1 - \frac{T_m}{T_h} \right) \right)^2} \right)^{\frac{1}{4}} \tag{41}$$

Equation 41 is potentially useful for sizing insulated structure. The structure could first be sized to carry the design structural loads. The resulting equivalent structural mass can then be compared to that calculated using Eq. 41. If the result of Eq. 41 is greater, then increasing the structural mass to that value will result in the lowest combined mass of structure and insulator. However, if the result of Eq. 41 is less, then adding additional structural mass will only increase the combined mass.

Substituting Eq. 41 back into Eq. 37 produces the following expression for the minimum mass of an insulated structure.

$$m_{opt} = (3 + 1) \, m_{so} \tag{42}$$

$$m_{opt} = 2 \left(\frac{2}{3}\right)^{\left(\frac{3}{4}\right)} \sqrt{t_h} \left(\frac{\left(\frac{\rho_e k_e}{\sqrt{c_{pe}}}\right)^2}{c_{ps} \left(-ln\left(1 - \frac{T_m}{T_h}\right)\right)^2}\right)^{\frac{1}{4}} \tag{43}$$

The first term in parentheses in Eq. 42 indicates the relative contributions of the insulation and structure, respectively, to the minimum total mass. For minimum total mass, Eq. 42 predicts that the mass of the insulation will be three times the mass of the structure. Eq. 43 defines the lower bound for the mass of an insulated structure subjected to a transient heat pulse. The magnitude of the minimum total mass is solely a function of the duration of the equivalent square heating pulse, t_h, and the figures of merit defined in Eqs. 39 and 40.

8   Analytical Predictions and Numerical Simulations

Several numerical studies were performed to assess how the simple approximate solutions derived in this paper compare to more accurate numerical simulations of Earth atmospheric entry heating on reusable launch vehicles. The objectives of the numerical studies were: 1) to assess the accuracy of using Eqs. 35 and 38 to size insulation for a realistic transient heating pulse, 2) to determine the applicability of the figures of merit defined by Eqs. 39 and 40 to results of atmospheric entry simulations, and 3) to investigate the interplay between the mass of the structure and the corresponding mass of insulation required to limit the maximum structural temperature.

The finite element model and heating histories previously described were used for all of these numerical studies. However, the finite element simulation was iterated to determine the insulation thickness required to limit the structural temperature rise to the specified value. Each transient simulation was continued until the structural temperature had reached its maximum value.

8.1   Thermal Properties of Structural Material

Obviously, raising the structural temperature limit will decrease the amount of required insulation. Less commonly considered is the effect of the structural specific heat capacity on the required insulation. Equation 39 defines a candidate figure of merit that combines the effects of structural temperature limit and specific heat capacity on the amount of required insulation.

A numerical study was performed to assess how well the results of a series of full numerical simulations would correlate to the parameter β_s. To compare the effects of the structural thermal properties, it was necessary to fix all other parameters in the problem and vary only the choice of structural material. LI-900 tile was chosen as the insulator and the structural mass per unit area was fixed at 6.10 $\frac{kg}{m^2}$ (1.25 $\frac{lbm}{ft^2}$). Two different heating histories were considered, but results can only be directly compared for a particular heating history. Table 10 shows thermal properties for four structural

Table 10. Thermal Properties of Four Structural Materials

$T_i + T_m$	$c_{ps}(T_{cs})$	$\beta_s(BP7940)$	$\beta_s(ATSpA)$
$K(°F)$	$\frac{J}{kgK}\left(\frac{Btu}{lbm°R}\right)$	$\frac{J}{kgK}\left(\frac{Btu}{lbm°R}\right)$	$\frac{J}{kgK}\left(\frac{Btu}{lbm°R}\right)$
Aluminum 2024 $\rho_s = $**2803** $\frac{kg}{m^3}$ **(0.10** $\frac{lbm}{in^3}$**)**			
422(300)	900(0.215)	27(0.006)	25(0.006)
450(350)	910(0.217)	41(0.010)	38(0.009)
Graphite/epoxy $\rho_s = $**1576** $\frac{kg}{m^3}$ **(0.057** $\frac{lbm}{in^3}$**)**			
366(200)	913(0.218)	9(0.002)	8(0.002)
422(300)	984(0.235)	30(0.007)	27(0.006)
Beryllium Aluminum $\rho_s = $**2098** $\frac{kg}{m^3}$ **(0.076** $\frac{lbm}{in^3}$**)**			
505(450)	1690(0.404)	151(0.036)	138(0.033)
561(550)	1735(0.415)	267(0.064)	244(0.058)
Titanium 6Al-4V $\rho_s = $**4437** $\frac{kg}{m^3}$ **(0.16** $\frac{lbm}{in^3}$**)**			
533(500)	574(0.137)	68(0.016)	62(0.015)
700(800)	594(0.142)	270(0.064)	242(0.058)

materials chosen for the study. The temperature dependent properties for these materials are tabulated in Reference [11]. The maximum allowable temperature for each material is application dependent, so an approximate upper and lower bound was chosen for each material. For each limiting temperature, the structural specific heat capacity (Eq. 30) and β_s for each of the two heating histories are shown in Table 10.

Iterative finite element analysis was used to size insulation for 16 cases (4 structural materials, 2 temperature limits, and 2 heating histories). The resulting insulation masses are shown in Fig. 19 and indicated by the square symbols. For the ATSpA heating history, each particular structural material and temperature limit is identified in the figure. The square symbols are not labeled for the BP7490 heating history to avoid cluttering the figure. The approximate insulation masses, calculated using Eq. 38, are indicated by circles corresponding to each of the 16 cases sized by the finite element solution. For the Space Shuttle heating history, BP7490, half of the approximate solutions are within 10% of the finite element solutions and all of the approximate solutions are within 25%. For the reusable launch vehicle heating history, ATSpA, half of the approximate solutions are within 10% of the finite element solutions and all of the approximate solutions are within 20%. Because the value of c_{pe} used in Eq. 38 is a function of the maximum structural temperature limit (Eq. 31), the approximate insulation masses are not solely a function of β_s. The solid lines in Fig. 19 represent the approximate solution using a value of c_{pe} that is an average of the 8 cases for each temperature history. The close agreement between the solid lines and circles indicates that, for LI-900 insulation, the variation
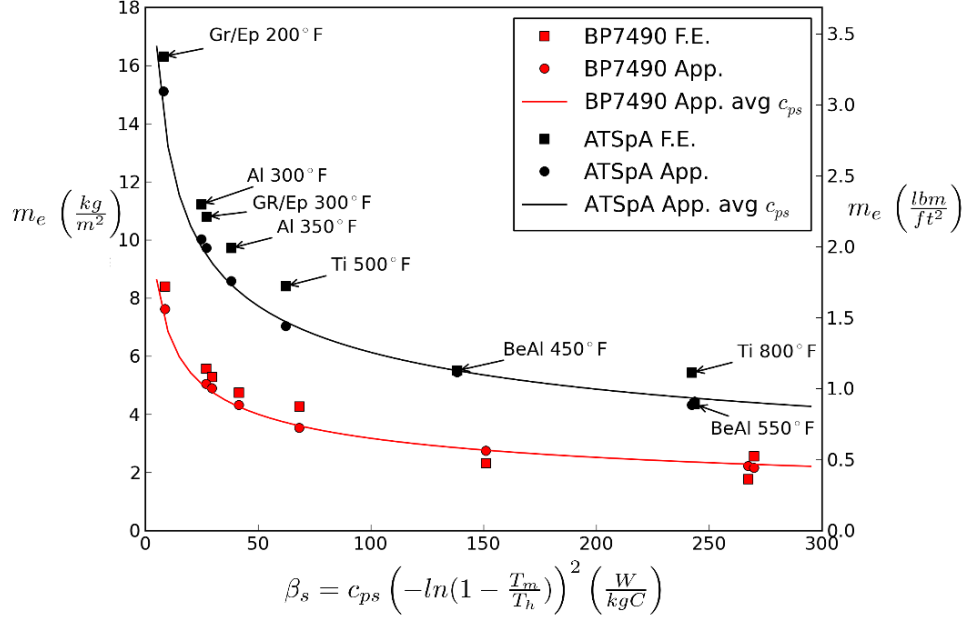
Figure 19. Effect of structural thermal properties on required insulator mass

of c_{pe} with T_m has little effect on the mass of required insulation. The solid lines clearly indicate the effect of β_s on the required insulation mass predicted by the approximate solution, Eq. 38. Remarkably, the finite element solutions closely follow this trend, even with four different structural materials. Therefore, the parameter β_s appears to be a useful indicator of the thermal effectiveness of a structural material.

8.2 Thermal Properties of Insulator

To better understand the significance of the parameter defined in Eq. 40, it is helpful to consider a range of candidate insulator materials that could be used for thermal protection on a reusable launch vehicle. A numerical study was performed to investigate the relative mass efficiency of a range of insulators for two different surface temperature histories (BP7490 and ATSpA) from Table 8. Five rigid ceramic tile materials (LI-900, LI-2200, FRCI-12, AETB-8, AETB-16) and four flexible insulations (Saffil-3, Saffil-6, Qfiber-3, and Qfiber-6) were considered. The temperature and pressure dependent thermal properties of the three Space Shuttle Orbiter tile materials ((LI-900, LI-2200, and FRCI-12) were obtained from published tables [4]. The thermal properties for AETB-8 and AETB-16 were calculated using the model developed by Daryabeigi [12] and the flexible insulation properties were calculated using the models also developed by Daryabeigi [7]. For this study, aluminum with a maximum temperature limit of 450K (350°F) was chosen as the underlying structure. The structural mass per unit area was fixed at 6.10 $\frac{kg}{m^2}$ (1.25 $\frac{lbm}{ft^2}$).

Table 11 shows the effective c_{pe} (Eq. 31) and k_e (Eq. 32) of each insulation for the two surface heating histories. The insulation figure of merit, calculated using

38

Eq. 40, is shown for each set of material properties. As shown in Table 11, the insulation effective material properties and figure of merit, κ_e, for a given insulation can be significantly different for different surface temperature histories. Therefore, insulations should be directly compared only for a given surface temperature history, structural material, and structural mass.

The iterative finite element analysis, previously described, was used to calculate the required insulation mass for each insulation and surface heating history listed in Table 11. Fig. 20 shows the required insulation masses versus the insulation figure of merit, κ_e. Each symbol shape represents the finite element solution for each of the insulations represented in Table 11 and the solid line represents the approximate solution calculated using Eq. 38. The red line and symbols correspond to the BP7490 temperature history and the black line and symbols correspond to the ATSpA temperature history. For each temperature history, the finite element results for this wide range of insulators clearly follow the trend predicted by the approximate solution.

For both surface temperature histories the flexible insulation materials are more mass efficient than the rigid tile materials. For the Shuttle Orbiter surface temperature history (BP7490), the bulk of the heating takes place at such a low pressure that gas conduction is not significant and radiation dominates the

Table 11. Insulation figure of merit values for aerospace insulations

Temp. History	c_{pe}	k_e	$\kappa_e = \frac{\rho_e k_e}{\sqrt{c_{pe}}}$
	$\frac{W}{mK}$	$\frac{J}{kgK}$	$\frac{kg^2}{m^3 s^2 \sqrt{K}}$
LI-900 $\rho_s =$**144** $\frac{kg}{m^3}$ (**9** $\frac{lbm}{ft^3}$)			
BP7490	949	0.03399	0.1589
ATSpA	949	0.06060	0.2832
LI-2200 $\rho_s =$**352** $\frac{kg}{m^3}$ (**22** $\frac{lbm}{ft^3}$)			
BP7490	949	0.06046	0.6907
ATSpA	949	0.08326	0.9512
FRCI-12 $\rho_s =$**192** $\frac{kg}{m^3}$ (**12** $\frac{lbm}{ft^3}$)			
BP7490	949	0.04039	0.2517
ATSpA	949	0.07212	0.4494
AETB-8 $\rho_s =$**128** $\frac{kg}{m^3}$ (**8** $\frac{lbm}{ft^3}$)			
BP7490	975	0.05702	0.2338
ATSpA	975	0.08728	0.3578
AETB-16 $\rho_s =$**256** $\frac{kg}{m^3}$ (**16** $\frac{lbm}{ft^3}$)			
BP7490	975	0.05927	0.4860
ATSpA	975	0.08975	0.7360
Saffil-3 $\rho_s =$**48** $\frac{kg}{m^3}$ (**3** $\frac{lbm}{ft^3}$)			
BP7490	975	0.04352	0.0669
ATSpA	975	0.07302	0.1123
Saffil-6 $\rho_s =$**96** $\frac{kg}{m^3}$ (**6** $\frac{lbm}{ft^3}$)			
BP7490	975	0.02420	0.0744
ATSpA	975	0.05489	0.1688
Qfiber-3 $\rho_s =$**48** $\frac{kg}{m^3}$ (**3** $\frac{lbm}{ft^3}$)			
BP7490	932	0.04106	0.0646
ATSpA	932	0.07328	0.1152
Qfiber-6 $\rho_s =$**96** $\frac{kg}{m^3}$ (**6** $\frac{lbm}{ft^3}$)			
BP7490	932	0.02158	0.0679
ATSpA	932	0.04975	0.1564

heat transfer through the insulation. Therefore the density of the flexible insulation (affects the length of gas conduction path) has little effect on the thermal performance, so that all four flexible insulations have nearly the same mass efficiency. Conversely, the bulk of the heating for the reusable launch vehicle surface temperature history (ATSpA) occurs at a higher pressure at which gas conduction through the insulation is significant. Therefore, the lower density flexible insulations are more mass efficient than the higher density flexible insulations. The lower density insulations are more efficient because at a given mass they are thicker and thus provide a longer path for gas conduction. For both surface temperature histories, lower density ceramic tiles tend to be more mass efficient than higher density tiles because heat transfer due to solid conduction becomes more significant with increased density. However, the denser LI-900 tile is more mass efficient than the AETB-8 tile.

The required insulation masses predicted by the approximate equation are within 15% of the finite element solutions.
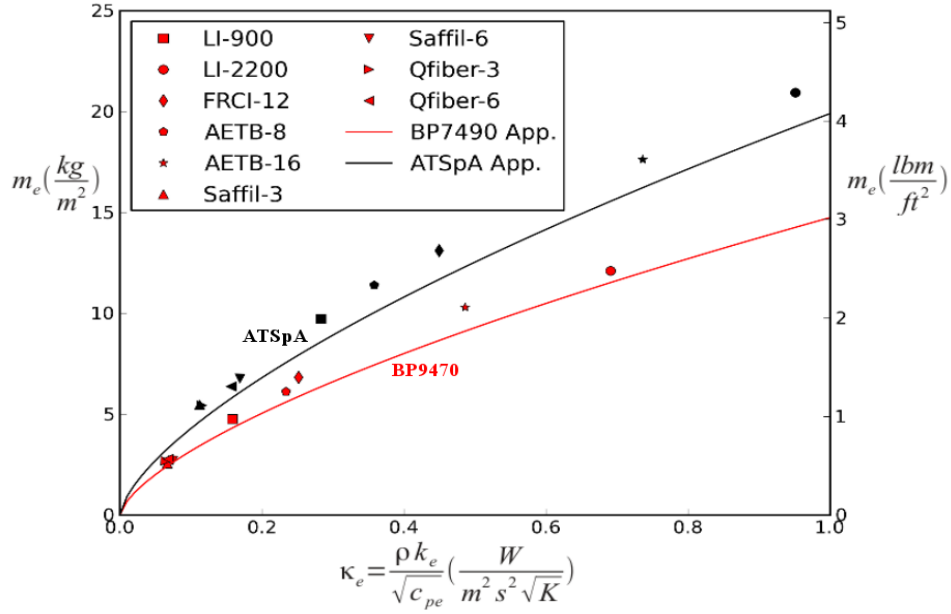

Figure 20. Required insulation mass for several insulators

8.3   Interplay Between Mass of Insulator and Structure

An additional numerical study was performed to gain a better understanding of the interplay between the mass of the structure and the mass of insulator required to limit the structural temperature. LI-900 ceramic tile was used as the insulator. Aluminum, with a maximum temperature limit of 450K ($350°F$), was chosen as the underlying structure. The structural mass per unit area was varied between 0.49 and 14.6 $\frac{kg}{m^2}$ (0.1 and 3.0 $\frac{lbm}{ft^2}$). For each of the two different surface temperature histories (BP7490 and ATSpA) from Table 8, iterative finite element analyses were performed for thirteen different values of structural mass per unit area to calculate the required insulation mass.

Results of this numerical study are shown in Fig. 21. The red symbols and lines correspond to the BP7490 heating history and the black to the ATSpA heating history. The blue line is the mass of the structure, which was the same for both heating histories. Required insulation masses calculated using the finite element analyses are represented by the solid circles. Dashed lines represent the corresponding approximate insulation masses calculated using Eq. 38 with properties defined by Eqs. 30-32. The solid squares represent the sum of the finite element solutions for insulation mass and the structural mass. The solid lines represent the sum of the approximate solution for insulation mass and the structural mass. The solid triangles represent the minimum total mass calculated using Eqs. 41 and 43.
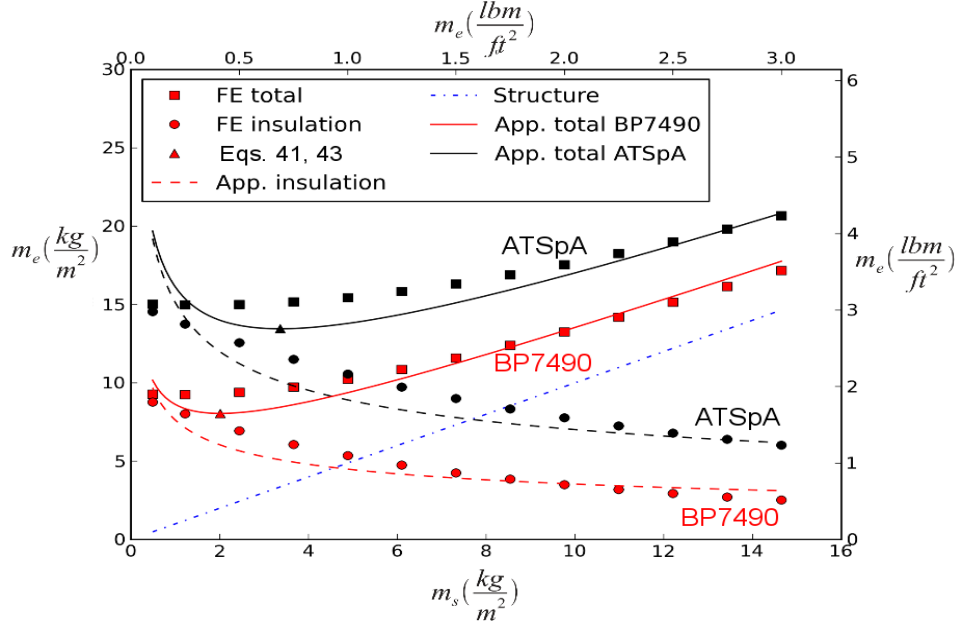
40

Figure 21. Mass of insulated structure as a function of structural mass

Comparison of the required insulation masses calculated using the finite element analysis and using Eq. 38 (solid circles vs dashed lines in Fig. 21) shows remarkably good agreement. Over the middle range of structural masses studied the approximate solution is within 15% of the finite element solution for both heating histories. However, for values of structural mass below 1 $\frac{kg}{m^2}$, the approximate solution begins to sharply diverge from the finite element solution. Also, at the high end of the range of structural masses, the approximate solution for the BP7490 heating history is beginning to diverge from the finite element solution. This indicates that the approximate solution may become much less accurate when the ratio of insulation mass to structural mass becomes very high or very low. The total mass is obtained by simply adding the structural mass to the insulation mass, so the accuracy comparison between the finite element and approximate solutions is similar to that for the required insulation masses.

As the structural mass increases, the required insulation mass decreases, so there is the potential for a combination of structure and insulator that produces the minimum total mass. For the finite element results, the total mass minimum occurs at a structural mass value of about 1 $\frac{kg}{m^2}$ (0.2 $\frac{lbm}{ft^2}$) for both heating histories. Equation 41 predicts a minimum at a structural mass of 2.1 $\frac{kg}{m^2}$ for the BP7490 heating history and 3.6 $\frac{kg}{m^2}$ for the ATSpA heating history. Although Eq. 41 does not accurately predict the structural mass at which the total mass is a minimum, the values of the minimum total mass predicted using Eq. 43 are within 10% of the finite element calculations for both heating histories. The three to one ratio of insulator mass to structural mass predicted to occur (Eq. 42) at the minimum mass appears to be an

41

artifact of error in the approximation.

The total mass curves in Fig. 21 are relatively flat over a significant range of structural masses. Therefore, the mass (and thickness) of the insulator can be reduced by increasing the structural mass, for a relatively modest total mass penalty. Thinner vehicle walls, insulator plus structure, could improve vehicle packaging efficiency, perhaps resulting in a net mass savings.

9   Conclusions

A simplified transient thermal problem was investigated in an attempt to gain basic insight into the thermal response of an insulated structure. A one-dimensional problem, consisting of a homogeneous insulator in perfect contact with an underlying, perfectly insulated structure was defined. From an initial uniform temperature, the outer surface of the insulator is instantaneously raised to an elevated temperature, held at that temperature for finite time, and then instantaneously returned to the initial temperature.

An analytical solution was derived for the transient response of this simplified transient problem. Although the solution is a rather unwieldy infinite series, the thermal response is completely governed by two nondimensional parameters with physical significance. Numerical examples were presented using properties and a heating duration representative of ceramic tiles on the Space Shuttle Orbiter.

The analytical series solution was used to calculate the maximum structural temperatures over a range of the two governing parameters. A simple function of the two governing parameters was constructed and used to approximate the maximum structural temperature over the selected range of the parameters. From this function, two approximate equations were developed for predicting the maximum structural temperature rise of an insulated structure.

Techniques were developed to choose a constant effective value for each of the temperature and pressure dependent material properties of the insulator and structural materials. A technique was also developed for defining an equivalent square heating pulse for a wide range of surface temperature histories associated with atmospheric entry. Analytical solutions for maximum structural temperature rise, using these constant effective material properties and simplified equivalent square heating pulses were compared to finite element solutions with variable material properties and time-accurate surface temperature histories for a range of insulator thicknesses. Results for the analytical series solution were typically within 10% to 20% of the finite element solutions. The approximate analytical solution had similar accuracy for many of the cases studied, but began to lose accuracy as one of the nondimensional governing parameters, the ratio of insulation heat capacity to structure heat capacity, became small.

Approximate analytical equations were developed for sizing the insulator thickness and mass required to maintain the insulated structural skin of hypersonic aerospace vehicles below a specified temperature. Manipulation of the equations revealed that the thermal properties of the insulator and of the structure could each be collected into a single term. These terms could be used as figures of merit to

42

indicate the effect of the choice of insulator or structural material on the required insulator mass. An equation was also developed for the minimum total mass of an insulated structure sized to stay below the maximum structural temperature limit, ignoring other design considerations.

A one-dimensional, finite element, transient thermal analysis was used to perform numerical studies for comparison with the results of approximate equations developed in this paper. The finite element analysis included the effects of temperature and pressure dependent material properties. Time-accurate surface temperature histories and ambient pressure histories were also incorporated into the numerical models.

A numerical study was performed to compare the mass of insulation required to protect four different structural materials. Two different maximum structural temperatures were considered for each structural material. The insulation material and the structural mass were kept the same. Calculations were performed for two different surface temperature histories. The approximate solution predicted the required insulation masses to within 10% of the finite element results for more than half of the cases and to within 25% for all of the cases considered. The finite element results exhibited a close correlation to the figure of merit, β_s, derived in this paper.

A second numerical study was performed to compare the mass efficiency of nine different aerospace insulators, five ceramic tile materials and four flexible insulations. The structural material, mass and maximum temperature limit were held constant while the required insulation masses were calculated for the same two surface temperature histories. For the insulations considered, the required insulation masses predicted by the approximate equation were within 15% of the finite element solutions. The finite element results were closely correlated to the insulation efficiency figure of merit, κ_e, derived in this paper.

A third numerical study was performed to investigate the effect of structural mass on the mass of required insulation and to determine the minimum mass for an insulated structure designed with only thermal constraints. The structural material and maximum temperature, as well as the insulation material, were held constant and the required insulation masses were calculated for a range of structural masses and for the same two surface temperature histories. For very small or very large values of structural mass the approximate solution diverges from the finite element solutions, however, away from these extremes the approximate solution was within 15% of the finite element solution. The approximate equation for minimum total mass was within 10% of the finite element solution, however, the approximate equation predicted the minimum total mass at a much larger value of the structural mass than the finite element solution.

The approximate equations developed in this paper were shown to predict the results of much more complex finite element calculations with surprising accuracy for the wide range of cases considered. Achieving these accurate results requires carefully following the techniques developed for mapping the transient surface temperature histories to equivalent square temperature pulses and for calculating the effective property values to use in the approximate equations. These simple approximate equations are useful for the preliminary investigation of a wide range of design

space to identify attractive regions for more detailed study. The figures of merit developed in this paper can also be helpful for choosing between available insulation and structural materials as well as providing guidance for developing more efficient materials. The successful development of constant, effective values for the temperature and pressure dependent thermal properties of monolithic insulators raises the intriguing possibility of developing effective properties for more complex sandwich cores or composite insulations for use in the simple approximations.

References

1. Gogu, C.; Haftka, R. T.; Bapanapalli, S. K.; and et. al.: Dimensionality Reduction Approach for Response Surface Approximations: Application to Thermal Design. *AIAA Journal*, vol. 47, no. 7, 2009, pp. 1700–1708.

2. Carslaw, H. S.; and Jaeger, J. C.: *Conduction of Heat in Solids*. Oxford University Press, Oxford, 1959. Second edition.

3. De Chant, L. J.: Analytical Solutions for Diffusive Finite Reservoir Problems Using a Modified Orthogonal Expansion Method. *Mathl. Comput. Modelling*, vol. 28, no. 11, 1998, pp. 73–86.

4. Williams, S. D.; and Curry, D. M.: Thermal Protection Materials: Thermophysical Property Data. NASA RP–1289, Dec. 1992.

5. Jones, E.; Oliphant, T.; Peterson, P.; and et.al: SciPy: Open Source Scientific Tools for Python. URL: http://www.scipy.org, 2001-2012.

6. Logg, A.; and Wells, G.: DOLFIN: Automated finite element computing. *ACM Transactions on Mathematical Software*, vol. 37, no. 2, 2010, p. 28.

7. Daryabeigi, K.; Cunnington, G. R.; Miller, S. D.; and Knutson, J. R.: Combined Heat Transfer in High-Porosity High-Temperature Fibrous Insulations: Theory and Experimental Validation. AIAA Paper 2010-4660, June 2010.

8. Gibson, D. M.; and et. al.: HYTHIRM Radiance Modeling and Image Analyses in Support of STS-119, STS-125 and STS-128 Space Shuttle Hypersonic Reentries. AIAA Paper 2010-244, Jan. 2010.

9. Zalameda, J. N.; and et. al.: Application of a Near Infrared Imaging System for Thermographic Imaging of the Space Shuttle during Hypersonic Re-Entry. AIAA Paper 2010-245, Jan. 2010.

10. Myers, D. E.; Martin, C. J.; and Blosser, M. L.: Parametric Weight Comparsion of Current and Proposed Thermal Protection System (TPS) Concepts. AIAA Paper 99-3459, June 1999.

11. Blosser, M. L.: Advanced Metallic Thermal Protection Systems for Reusable Launch Vehicles. Ph.D. dissertation, University of Virginia, Charlottesville, VA, May 2000.

12. Daryabeigi, K.; Cunnington, G. R.; and Knutson, J. R.: Heat Transfer Modeling for Rigid High-Temperature Fibrous Insulation. AIAA Paper 2012-3004, June 2012.

Appendix A

Derivation of Series Solution

In Reference [3] De Chant derives the solution to a problem that is similar to the second portion of the current problem, $t > t_h$. De Chant's solution is for a uniform initial temperature distribution with the outer surface temperature of the insulator instantaneously reduced to zero. A solution to the same problem is presented in Reference [2], but it appears to be incorrect – as noted by De Chant and verified in the current effort.

In Reference [3] De Chant defines the following problem (converted to the nomenclature of the current paper) to be solved.

$$\frac{\partial T}{\partial t} = \beta \frac{\partial^2 T}{\partial^2 x} \tag{A-1}$$

with the boundary condition at $x = 1$ as

$$\frac{\partial T(1,t)}{\partial t} = -\beta\gamma \frac{\partial T(1,t)}{\partial x} \tag{A-2}$$

the boundary condition at $x = 0$ as

$$T(0,t) = 0 \tag{A-3}$$

and the initial condition as

$$T(x,0) = T_{io} \tag{A-4}$$

The dimension d_e appears, indirectly through β, in Eqs. A-1 and A-2 as a result of nondimensionalizing the spatial variable x.

De Chant then separates variables to get a first order ordinary differential equation in time that can be readily solved to obtain an exponential decay term and an eigenvalue problem in the spatial variable.

$$\phi''(x) + \lambda^2 \phi'(x) = 0 \tag{A-5}$$

The eigenfunctions that solve Eq. A-5 are given by

$$\phi_n(x) = \sin(\lambda_n x) \tag{A-6}$$

and the eigenvalues can be obtained by solving Eq. 15.

The boundary condition at $x = 1$ causes some difficulty in proceeding with the solution. De Chant overcomes this difficulty by developing a "weighting" function.

$$\sigma(x) = 1 + \frac{1}{\gamma}\delta(x - 1) \tag{A-7}$$

where δ denotes the Dirac delta function.

The weighting function is then used to ensure orthogonality of the eigenfunctions.

$$\int_0^1 \phi_i(x)\phi_j(x)\sigma(x)dx = 0 \tag{A-8}$$

The next step in the solution is to satisfy the initial condition by using an eigenvalue expansion.

$$\frac{T_o(x)}{T_h} = \sum_{n=1}^{\infty} b_n \phi_n(x) \tag{A-9}$$

However, rather than using a uniform temperature distribution for the initial condition of the second part of the problem, the temperature distribution from Eq. 13 at time $\tau = \tau_h$ is used as the initial condition.

$$\frac{T_o(x)}{T_h} = 1 - \sum_{m=1}^{\infty} c_m \sin(\lambda_m x) e^{-\lambda_m^2 \tau_h} \tag{A-10}$$

Application of the orthogonality relationship, Eq. A-8, yields

$$b_n = \frac{\int_0^1 \frac{T_o(x)}{T_h} \phi_n(x)\sigma(x)dx}{\int_0^1 \phi_n^2(x)\sigma(x)dx} \tag{A-11}$$

Substituting Eqs. A-6 and A-7 into Eq. A-11 and applying the Dirac delta function produces

$$b_n = \frac{\int_0^1 \frac{T_o(x)}{T_h} \sin(\lambda_n x)dx + \frac{1}{\gamma}\frac{T_o(1)}{T_h}\sin\lambda_n}{\int_0^1 \sin^2(\lambda_n x)dx + \frac{\sin^2\lambda_n}{\gamma}} \tag{A-12}$$

Further substitution of Eq. A-10 into Eq. A-12 and rearranging terms gives

$$b_n = \frac{\left(\int_0^1 \sin(\lambda_n x)dx + \frac{\sin\lambda_n}{\gamma}\right) - \sum_{m=1}^{\infty}\left(\int_0^1 c_m \sin(\lambda_m x)\sin(\lambda_n x)dx + c_m \sin\lambda_m \sin\lambda_n\right)e^{-\lambda_m^2\tau_h}}{\int_0^1 \sin^2(\lambda_n x)dx + \frac{\sin^2\lambda_n}{\gamma}} \tag{A-13}$$

Integrating Eq. A-13 produces

$$b_n = \frac{\left(\frac{1-\cos\lambda_n}{\lambda_n} + \frac{\sin\lambda_n}{\gamma}\right) - \sum_{m=1}^{\infty}\left(\frac{\lambda_n \sin\lambda_m \cos\lambda_n - \lambda_m \sin\lambda_n \cos\lambda_m}{\lambda_m^2 - \lambda_n^2} + \frac{\sin\lambda_m \sin\lambda_n}{\gamma}\right)c_m e^{-\lambda_m^2\tau_h}}{\frac{1}{2} - \frac{\sin(2\lambda_n)}{4\lambda_n} + \frac{\sin^2\lambda_n}{\gamma}} \tag{A-14}$$

The first term in the numerator represents the solution for the uniform initial temperature problem. It can be shown to be the same as the coefficients defined in Eq. 14. Using this observation and trigonometrical identities for the product of sine and cosine, Eq. A-14 can be rewritten as

$$b_n = c_n - \frac{\sum_{m=1}^{\infty} \left(\frac{\sin(\lambda_n - \lambda_m)}{\lambda_n - \lambda_m} - \frac{\sin(\lambda_n + \lambda_m)}{\lambda_n + \lambda_m} + \frac{2\sin\lambda_m \sin\lambda_n}{\gamma} \right) c_m e^{-\lambda_m^2 \tau_h}}{1 - \frac{\sin(2\lambda_n)}{2\lambda_n} + \frac{2\sin^2\lambda_n}{\gamma}} \qquad \text{(A-15)}$$

Inspection of Eq. A-15 reveals a potential numerical problem when $m = n$. The first term in the large parentheses of Eq. A-15 approaches 1 in the limit as $\lambda_m \to \lambda_n$. Therefore, for $n = m$ the quantity in the large parentheses becomes equivalent to the denominator and cancels out. Eq. A-15 can thus be rewritten as

$$b_n = c_n(1 - e^{-\lambda_n^2 \tau_h}) - \sum_{\substack{m=1 \\ m \neq n}}^{\infty} \left(\frac{\frac{\sin(\lambda_m - \lambda_n)}{(\lambda_m - \lambda_n)} - \frac{\sin(\lambda_m + \lambda_n)}{(\lambda_m + \lambda_n)} + \frac{2\sin\lambda_m \sin\lambda_n}{\gamma}}{1 - \frac{\sin(2\lambda_n)}{2\lambda_n} + \frac{2\sin^2\lambda_n}{\gamma}} \right) c_m e^{(-\lambda_m^2 \tau_h)}$$

$$\text{(A-16)}$$

which is the same as Eq. 17. A simple offset in the time variable completes the solution shown in Eq. 16.

Appendix B

Material Properties

Table B1. Properties for aluminum 2024 (Ref. [4])

Temperature	c_p	k
$^\circ R(K)$	$Btu/lbm/^\circ R(J/kg/K)$	$Btu/ft/hr/^\circ R(W/m/K)$
160 (89)	0.177 (741)	61.2 (106)
260 (144)	0.147 (615)	69.6 (120)
460 (256)	0.195 (816)	84.0 (145)
660 (367)	0.216 (904)	95.0 (164)
760 (422)	0.224 (937)	99.0 (171)
860 (478)	0.233 (975)	102.5 (177)
1060 (589)	0.250 (1046)	104.5 (181)

Table B2. Specific heat capacity for LI-900 (Ref. [4])

Temperature	c_p
$^\circ R(K)$	$Btu/lbm/^\circ R(J/kg/K)$
460 (256)	0.150 (628)
710 (394)	0.210 (879)
960 (533)	0.252 (1054)
1210 (672	0.275 (1151)
1460 (811)	0.288 (1205)
1710 (950)	0.296 (1238)
1960 (1089)	0.300 (1255)
2210 (1228)	0.303 (1268)
2460 (1367)	0.303 (1268)
3460 (1922)	0.303 (1268)

Table B3. Thermal conductivity for LI-900 (Ref. [4])

T, °R	k, Btu/(ft hr °R)					
	Pressure, atm					
	0	0.0001	0.001	0.01	0.1	1.0
460	0.0075	0.0075	0.0100	0.0183	0.0250	0.0275
710	0.0092	0.0092	0.0125	0.0225	0.0316	0.0341
960	0.0125	0.0125	0.0167	0.0276	0.0400	0.0433
1210	0.0175	0.0175	0.0216	0.0325	0.0492	0.0534
1460	0.0233	0.0233	0.0275	0.0392	0.0600	0.0658
1710	0.0308	0.0308	0.0350	0.0492	0.0725	0.0782
1960	0.0416	0.0416	0.0459	0.0617	0.0875	0.0942
2210	0.0567	0.0567	0.0610	0.0767	0.1060	0.1130
2460	0.0734	0.0734	0.0782	0.0942	0.1270	0.1360
2760	0.0966	0.0966	0.1020	0.1160	0.1550	0.1670
2960	0.1660	0.1660	0.1230	0.1390	0.1790	0.1940
3260	0.1540	0.1540	0.1620	0.1800	0.2220	0.2420
3460	0.1900	0.1900	0.1960	0.2190	0.2620	0.2900

REPORT DOCUMENTATION PAGE

Form Approved
OMB No. 0704-0188

1. REPORT DATE *(DD-MM-YYYY)* 01-08-2012	2. REPORT TYPE Technical Publication	3. DATES COVERED *(From - To)*

4. TITLE AND SUBTITLE

Analysis and Sizing for Transient Thermal Heating of Insulated Aerospace Vehicle Structures

5a. CONTRACT NUMBER

5b. GRANT NUMBER

5c. PROGRAM ELEMENT NUMBER

6. AUTHOR(S)

Blosser, Max L.

5d. PROJECT NUMBER

5e. TASK NUMBER

5f. WORK UNIT NUMBER
736466.01.08.07.09.02

7. PERFORMING ORGANIZATION NAME(S) AND ADDRESS(ES)

NASA Langley Research Center
Hampton, VA 23681-2199

8. PERFORMING ORGANIZATION REPORT NUMBER

L-20165

9. SPONSORING/MONITORING AGENCY NAME(S) AND ADDRESS(ES)

National Aeronautics and Space Administration
Washington, DC 20546-0001

10. SPONSOR/MONITOR'S ACRONYM(S)

NASA

11. SPONSOR/MONITOR'S REPORT NUMBER(S)

NASA/TP-2012-217595

12. DISTRIBUTION/AVAILABILITY STATEMENT

Unclassified - Unlimited
Subject Category 34
Availability: NASA CASI (443) 757-5802

13. SUPPLEMENTARY NOTES

14. ABSTRACT

An analytical solution was derived for the transient response of an insulated structure subjected to a simplified heat pulse. The solution is solely a function of two nondimensional parameters. Simpler functions of these two parameters were developed to approximate the maximum structural temperature over a wide range of parameter values. Techniques were developed to choose constant, effective thermal properties to represent the relevant temperature and pressure-dependent properties for the insulator and structure. A technique was also developed to map a time-varying surface temperature history to an equivalent square heat pulse. Equations were also developed for the minimum mass required to maintain the inner, unheated surface below a specified temperature. In the course of the derivation, two figures of merit were identified. Required insulation masses calculated using the approximateequation were shown to typically agree with finite element results within 10%-20% over the relevant range of parameters studied.

15. SUBJECT TERMS

Insulated structure; Insulation; Thermal analysis; Thermal protection system

16. SECURITY CLASSIFICATION OF:			17. LIMITATION OF ABSTRACT	18. NUMBER OF PAGES	19a. NAME OF RESPONSIBLE PERSON STI Help Desk (email: help@sti.nasa.gov)
a. REPORT	b. ABSTRACT	c. THIS PAGE			19b. TELEPHONE NUMBER *(Include area code)*
U	U	U	UU	55	(443) 757-5802

Standard Form 298 (Rev. 8-98)
Prescribed by ANSI Std. Z39.18